Technische Universität München

Università degli Studi di Cagliari

Characterization of a hybrid gas detector with GEM + Micromegas Read Out

DEPARTMENT OF PHYSICS - Dense and Strange Hadronic Matter

Bachelor's thesis

25.11.2021

Reviewers:

Laura Fabbietti

Alessandro De Falco

Author:

Rossana Facen

Abstract

This work summarizes the principal results obtained studying a GEM - Micromegas detector.
Space charge distortion due to the accumulation of positive backflowing ions, and the occurrence of electrical discharges, are critical issues for gaseous detectors, such as GEMs and Micromegas. In order to partially overcome these problems, a hybrid GEM - Micromegas detector has been assembled and studied. The setup has been realized with a bulk Micromegas and a Standard GEM. To perform a comparative study, the Standard GEM has been then substituted with a Large Pitch one.
Taking into account the features of the detectors, the GEM foil has been used as a preamplifier stage, significantly decreasing the working voltage of the Micromegas. For the same voltage, the gain of the hybrid detector results amplified by a factor of ≈ 10, compared to the single Micromegas setup.
The optimal operational region of the detector, according to Hydra experiment requirements, is characterized by ion backflow $< 1\%$ and energy resolution $< 12\%$. This configuration has been achieved even at low voltages, preventing the occurrence of discharges.
Here it is reported the investigation of the detector performance in terms of gain, ion backflow and energy resolution, for different voltage configurations.

Contents

1 Introduction

The performance and accuracy of particle detectors has become an issue of fundamental importance in the high-energy physics field.
Nowadays, one of the most used types of detectors are the so called *gaseous ionization detectors*, based on the capability of charged particles to ionize gas [1; 2]. Here, an incident ionizing particle enters the detector chamber filled with a gas mixture (usually a noble gas and a quencher), and, if it has enough energy, it ionizes the surrounding atoms, creating electron-ion pairs.

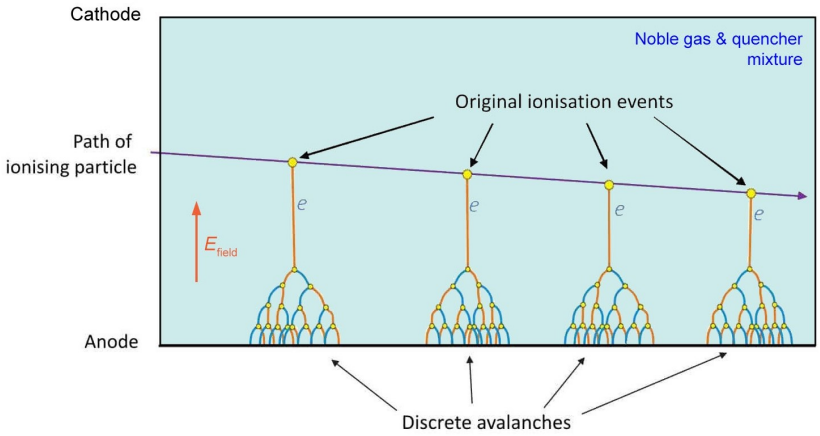

Figure 1: Scheme of a gaseous ionization detector, which in this case is capable of amplifying the original signal through avalanches.

With the presence of an external electric field, the resulting electrons and ions don't recombine, but flow to opposite directions. By the application of suitable voltages, it is possible to amplify the original signal: free electrons get accelerated, collide with gas atoms or molecules, and free more electrons. These secondary electrons are in turn accelerated, creating an avalanche multiplication, called *Townsend avalanche*. The ratio between the number of electrons created in avalanches at the distance x, $N(x)$, and the primary electrons N_0, is referred to as the detector *gain* G. According to experimental results, G can also be expressed as a function of the distance x:

$$G = \frac{N(x)}{N_0} = e^{\alpha \cdot x} \tag{1}$$

Where α represents the first *Townsend ionisation coefficient*, expressing the number of electrons generated per unit length by a single electron moving from cathode to anode, in a given electric field. At very high voltages, instead of a single localized avalanche, a chain reaction of many avalanches can spread out, causing a breakdown event, the *discharge* [3]. This process is mostly caused by ultraviolet photons emitted by deexciting molecules, which travel to other parts of the chamber, and cause further ionization. In order to stop the discharge, a quenching gas must be present in the medium, to absorb the photons and drain their energy into other channels. Polyatomic gases (such as CH_4 or CO_2) fulfill this criteria, since they have a number of closely spaced vibrational and rotational energy levels.
As it will be further discussed, other processes can give rise to discharges. Considering that they may cause severe damages to the detector, and to the readout system connected to the anode, discharges are to be avoided by all means.

Traditional radiation detectors, as Multi-Wire Proportional Chamber (MWPCs), consist of a parallel anode array of wires at high voltage, between two cathode planes at ground potential. Charge amplification is not necessarily confined to proportional wires though: it has been recently shown that Micropattern Gaseous Detectors, such as *GEM* or *Micromegas* detectors, can overcome most of the problems MWPCs have to deal with [4]. These high granularity gaseous detectors, manufactured by using microelectronic techniques, are characterized by a small distance (usually below 1 mm) between the anode and the cathode electrodes. Among the other advantages over wire detectors, there is especially the higher count rate capability.

1.1 Ion backflow and energy resolution

One critical issue of gas detectors at high flux, is the space charge distortion due to the accumulation of positive ions. After being created in avalanches, slow-moving positive ions drift from the amplification region to other parts of the gas chamber: this effect is known as *ion backflow*. The ion backflow is usually defined as the ratio of current measured on the cathode, over the anode current, or in term of the of the gain G:

$$IBF = \frac{I_{\text{cathode}}}{I_{\text{anode}}} = \frac{1+\epsilon}{G}, \tag{2}$$

where ϵ is the number of ions drifting back from the amplification to the drift region, per incoming electron [5]. Hence, the IBF depends mostly on the electrodes geometry and on fields strength.
Ion backflow has to be limited, to avoid the distortion of the local electric field, which may affect the ionizing electron's trajectories.

The energy delivered by an ionizing particle, is related to the number of charges produced: knowing the latter, one can determine the intrinsic spread in the energy deposited by the incident radiation [6]. The *energy resolution* specifies the best possible resolution that a system can have. Usually there are other factors to take into account, such as the noise and the resolving power of the associated electronics, that may deteriorate the resolution. The computation of this parameter depends mostly on which distribution the energy seems to follow: in the case of a perfect Gaussian function, its value can be determined knowing the position of the central peak μ_{peak}, and the standard deviation σ_{peak}:

$$E_{\text{res}} = \frac{\sigma_{\text{peak}}}{\mu_{\text{peak}}} \tag{3}$$

The energy resolution is one of the most important factors for an ionization detector: it characterizes the detector in terms of how well it can differentiate between closely spaced energy peaks in the spectrum, allowing us to understand its physical limits.

1.2 Gas Electron Multiplier (GEM)

A *Gas Electron Multiplier* detector, or *GEM*, is an ionization detector developed in 1997, by Fabio Sauli, at CERN [7].
The electrode of the device is a thin polyimide foil (usually made of Apical), copper-coated on both sides, and perforated with a high density of electrochemically etched holes. Because of the etching process, the holes are usually double-conical in shape, with wider diameter on the entry sides: this geometry helps improving dielectric rigidity, and reaching high gains [7; 8].
A Standard GEM has holes with outer and inner diameter of 70 μm and 50 μm respectively, hole pitch of 140 μm, thickness of 50 μm, and a copper thickness of 5 μm.

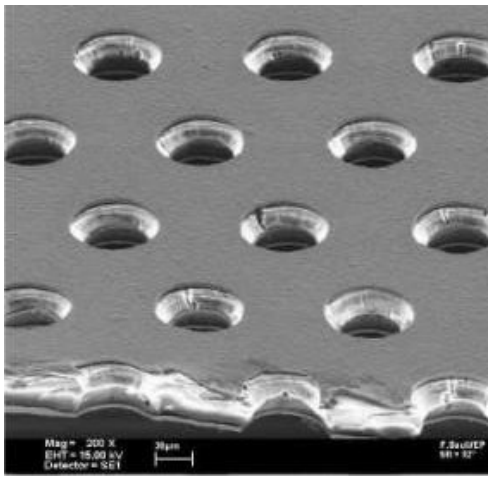

Figure 2: Electron microscope picture of a section of a Standard GEM foil.

In a detector setup, the GEM is inserted between a drift cathode, and a charge collection anode. The region between cathode and the top of the GEM is called *drift* region, since the electrons and ions produced after ionization drift to the respective electrodes. The charges amplification occurs on the other hand between the top and the bottom of the GEM foil. Applying a high voltage ($\approx 300 \div 400$ V) between the two sides of the GEM, a dipole field is formed, with an intensity of about 50 kV/cm. Because of the geometry of the device, the electric field in the holes is very intense, and it is able to focus electrons inside the gaps.
As an ionizing particle interacts with the gas of the chamber, electrons in the drift region are created. They then drift towards the GEM, and, once inside a hole, they get accelerated, causing an avalanche (see schematic representation in Figure 3b). A single electron entering a hole is multiplied by a factor from 10 to 1000, depending on the applied voltage.
All the field lines from the drift region enter the holes (Figure 3a): the fraction of electrons collected in GEM holes, the so called *collection efficiency* is thus close to 100%. On the other hand, the fraction of electrons extracted out of GEM holes, is usually referred to as *extraction efficiency*. Due to dispersing effects, part of the electrons produced within the holes reach the bottom side of the GEM, where they are neutralised. The rest of them can be extracted towards the readout anode, inducing a current signal, which can be measured by the readout electronics.
After being produced in the holes, the secondary electrons can also be injected into another multiplying region. A unique feature of GEMs is the possibility to pile stacks: with a proper choice of the fields, the fraction of amplified electrons can be injected and multiplied in a second foil, and yet again, up to five multipliers [7]. With a stack composed of three GEMs, for instance, a gain of the order of 10^4 can be easily attained, and each electrode can run at lower voltage, thus being much less prone to discharges. After an optimization of the gain share among the GEMs, the drift of positive ions emerging from next stages can be mostly blocked. As a matter of fact, GEMs stacks have been proven to be a very suitable technology for the upgrade of ALICE TPC (Time Projection Chamber), where ions returning to the drift region should be minimized to avoid distortions of the electric field in the drift volume [5].
Similar results can be achieved with a multistage gas electron multiplier, consisting of a GEM combined with another kind of ionization detector.
The GEM is only an amplification stage: it is independent of the readout structure, which can be optimized according to the application.

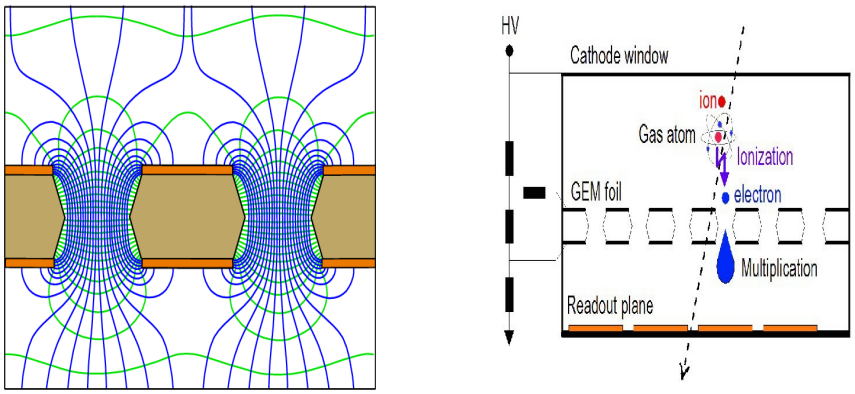

(a) Field lines of GEMs, close to holes.

(b) Electrons creation and multiplication.

Figure 3: Scheme of electric field lines close to GEM holes (a), and scheme of ionization process in a gas ionization chamber, with a GEM detector (b).

With multi-wire proportional chambers, the common way to minimise the ion backflow is the so called *gating grid* which, in turn, limits the maximum rate of MWPCs [9]. In GEM detectors, the ions created in the avalanches follow the electric field lines, because of their low velocity: a substantial part of them is collected on the top side of the GEM foil, causing an ion feedback of the order of $\approx 10\%$, similarly to MWPC. In the case of stacks, on the other hand, IBF is suppressed thank to the upper stages, which stop ions: the device offers intrinsic suppression of backdrifting ions, with $IBF \approx 0.1 \div 1\%$.
GEMs have recently been studied to understand their properties in the detection of soft X-rays and charged particles. It has been discovered that these detectors have many advantages such as excellent spatial resolution, toleration of high counting rate, and easy assembly. They are also more cost-efficient to produce, and maintain, as well as more robust to handle than MWPCs.

1.3 Micro-Mesh Gaseous Structure (Micromegas)

A Micro-Mesh Gaseous Structure (Micromegas or MMG), is a type of Micropattern Gaseous Detector, invented in 1995 by I. Giomataris and collaborators [10].
The MMG is a thin mesh, operated in parallel plate geometry, and placed between the drift and the amplification region of an ionization gas chamber. A gap of about 100 µm is kept between the mesh and the anode, by insulating pillars fabricated with photolithography, 50 µm thick. Applying the appropriate voltages on the three electrodes (cathode, mesh, anode), this configuration allows to get a high electric field in the amplification region ($\approx$ 100 kV/cm) and a low electric field in the drift volume.
Many different technologies have been developed for making meshes: they can be made of a thin metallic sheet, with a thickness of about $4 \div 10$ µm, and a typical pitch of 500 Lines Per Inch (LPI). In this case, the holes are usually electroformed, or chemically etched. On the other hand, MMG can also be made of woven stainless-steel, with wires of 18 µm, and a maximum mesh thickness of 30 µm [11].
Due to the very large field ratio between the drift and amplification regions (usually ≈ 400) and to the periodic pattern, the field lines from the drift region are compressed close to the MMG holes, forming a funnel. Therefore, an electron approaching the mesh is focused towards the center of a hole and produces an avalanche inside the funnel, which, due to the transverse diffusion, can also extend outside (in GEM, cascades are strictly confined inside the holes).

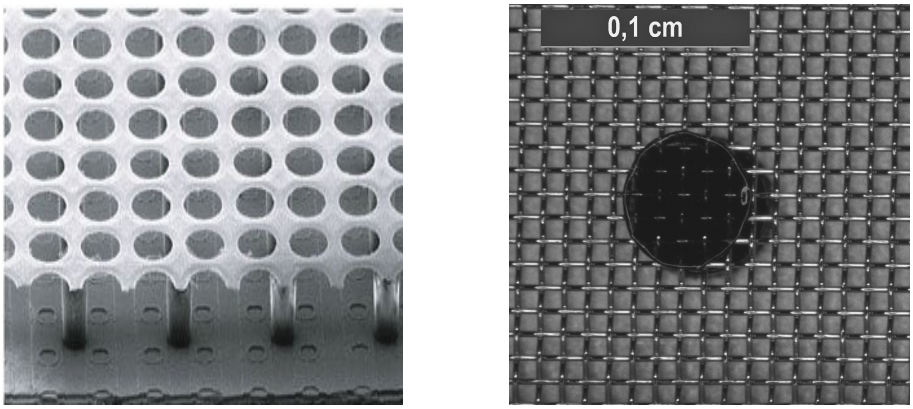

(a) Electroformed MMG. (b) Woven-like MMG.

Figure 4: Microscope pictures of two types of Micromegas. Insulating pillars can be seen below the mesh.

Most of the backdrifting ions from the amplification region, following the electric field lines, are collected by the mesh, and only a fraction of them flow back to the drift region. From these considerations, and knowing the size of the ion cloud and the mesh pitch, it is possible to calculate the ion feedback as a function of the fields ratio, finding that $IBF \propto E_{\text{drift}}/E_{\text{MMG}}$ [12].

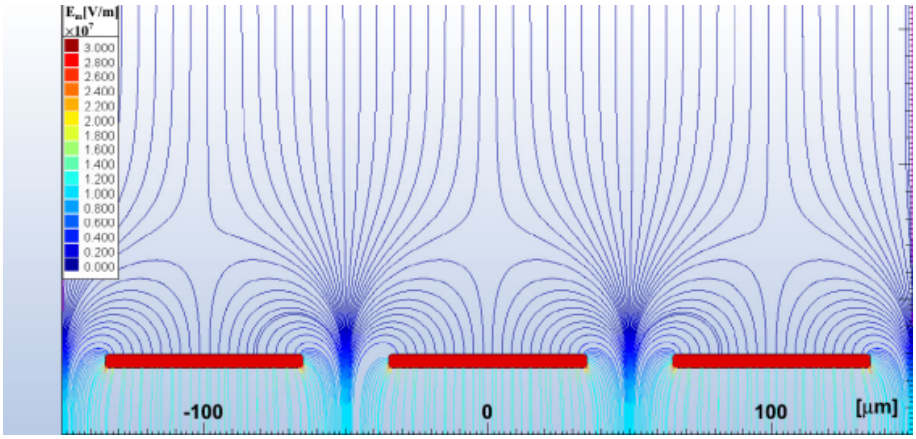

Figure 5: Field lines close to a Micromegas detector.

In *Bulk Micromegas*, mesh, pillars, and the readout structure form one single entity: the pillars are attached to the anode, and in turn the mesh is encapsulated inside the pillars. Most detectors are manufactured using this method, because they result robuster and can withstand several sparks before being damaged.
Along with excellent time and spatial resolution, MMG has been known to be very radiation hard and robust in high intensity radiation. Moreover, Micromegas detectors have a higher ion suppression capability than GEMs, due to their geometric and electrostatic configuration.

1.4 GEM - Micromegas detector

Despite their numerous advantages, GEM and Micromegas detectors have to deal with some issues that were not discussed so far, mostly related with discharges.
In the cascade of GEMs, the last GEM foil (near to the anode), can be easily damaged, because of the large number of electrons created in avalanches. If the charges produced in cascades exceed a certain limit (called *Raether limit* [13]), a spark may develop, causing in turn damages to the detector, or dead times. Similarly, at very high voltages, the MMG starts being particularly vulnerable to sparks and discharges, even when a large dead time is introduced.
To decrease the sparking probability, a GEM-Micromegas detector can be built and studied. Any electron created in the ionization process will experience two amplifications: first GEM, and then Micromegas. The MMG provides most of the gain, and can be thus operated at low voltages, since the GEM works as a preamplifier stage. With this configuration, it can be shown that the sparking rate is reduced by a factor of 100, while obtaining the same or higher gain than the single-Micromegas setup [14].
Another advantage is that most ions are collected by the GEM, preventing them from entering the drift region.
The gaps between GEM and MMG, and between MMG and anode, are called *transfer* and *amplification* regions respectively. The ratio between the amplification and the transfer field, $E_{\text{ampl}}/E_{\text{tr}}$ is of fundamental importance: it has to be high (usually ≥ 10), in order to reach 100% of Micromegas extraction efficiency. Since the increase of E_{ampl} implies the increment of spark probability, E_{tr} is usually kept low. On the other hand, the GEM extraction efficiency increases with the ratio $E_{\text{tr}}/E_{\text{GEM}}$: if E_{tr} is too small, electrons amplified in the first stage will be collected by the GEM lower part, and only a small number of electrons will be extracted towards the MMG. The number of electrons lost to either device, influences both the gas gain and the shape of the energy spectrum [15].
Regarding the GEM collection efficiency, it decreases with the ratio $E_{\text{drift}}/E_{\text{GEM}}$.
For this kind of detector, the ion feedback depends on the field ratios between the drift, transfer and amplification region, while the energy resolution is mostly determined by the first amplification stage, the GEM, and only weakly depends on the MMG. As far as ion backflow and E_{res} are concerned, the performance of GEM-Micromegas detector can be compared to the 4-GEMs stack configuration [16].
Due to the presence of a quencher, the discharges are not mainly caused by ultraviolet photons. The principal source of spark is instead the accumulation of charges in GEM holes, when they exceed the Raether limit of $10^6 \div 10^7 e$ [17].

The implementation of GEM - Micromegas device can be considered advantageous for the upgrade of large trackers used in many ongoing experiments.
For instance, the *Hydra experiment* [18], which performs hypernuclear studies with a TPC in R3B, plans to use such a hybrid detector in future, to perform measurements. In particular, the experiment requires an *IBF* less than 1%, energy resolution $< 15\%$, for a gain of 5000.
The main goal of this work is therefore the investigation of the principal properties of a GEM - Micromegas detector, in order to find out if these and other operational requirements can be achieved. For the optimization of the device, fields and voltages have been tuned, gradually measuring gain, ion backflow, and energy resolution.

2 Experiment

2.1 Experimental setup

The hybrid detector setup is schematically shown in Figure 6.
The gas used for the entire experiment is a mixture of Ar and CO_2 (the latter acting as a quencher), in proportion of 90-10. The gas flow has been most of the time 10 l/h.
For the first measurements, an α source of ^{241}Am + ^{244}Cm + ^{239}Pu, with a rate of 525 Hz has been used. The source has been fixed with Kapton tape on top of the PCB cathode, shooting through a 7 mm diameter hole. The energy of the α particles can be calculated as the weighted average of 5.486 MeV from ^{241}Am, 5.805 MeV from ^{244}Cm, and 5.155 MeV of ^{239}Pu.
Later, for energy resolution studies, the α source has been replaced with ^{55}Fe, an X-ray source with emitting energy of 5.9 keV, and rate of 121 kHz. The evaluation of energy resolution by using ^{55}Fe is much more precise. Before being completely stopped, the α particles can travel in the gas medium for a length in the order of cm: they may escape the gas chamber, without releasing their entire energy. An X-ray photon, on the contrary, excite immediately some electron of the gas, which is freed, and can travel only for $\approx$ 100 µm, before ionizing other atoms: X-ray sources thus are much more efficient than α ones for energy resolution studies.
Basing on precedent researches, the drift and the transfer gaps were chosen of 20 mm and 4 mm respectively [16]. GEM and MMG have been connected to the power supply via a 4.7 MΩ resistor, in order to protect the detectors from any damage during discharges. With such configuration, four different parameters can be changed: the electric field in the drift region, E_{drift}; the voltage between GEM top and GEM bottom, ΔV_{GEM}; the field in the transfer region, E_{tr}; the voltage between Micromegas and anode, ΔV_{MMG}. The values of these variables have been controlled via LabView software.

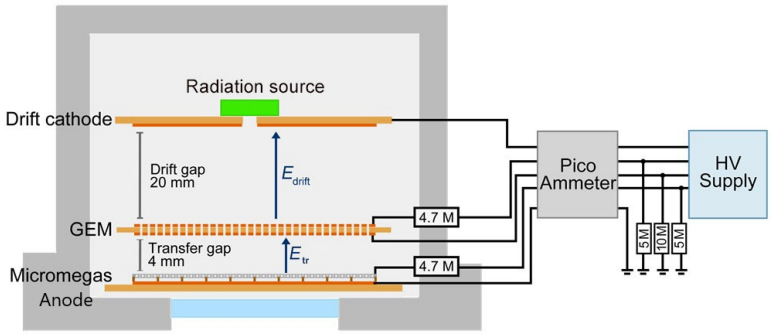

Figure 6: Scheme of the hybrid GEM - Micromegas detector.

The detectors used have an active area of 10×10 cm^2.
Two GEMs with different hole pitches were studied: the *Standard* GEM with the specifics described in Section 1.2, and a *Large Pitch* GEM (LP GEM) with hole pitch of 280 µm. The MMG used is a woven-type Bulk Micromegas, with an amplification gap 128 µm wide, pitch wire of 640 LPI, and wires 13 µm thick. GEM and Micromegas were produced at CERN, by MPT laboratory [19].
After the assembly, the stack of detectors has been placed into a gas tight vessel, connected with the HV power supply, and gas pipes. For safety reason, the vessel has been in turn put inside a copper shield box.

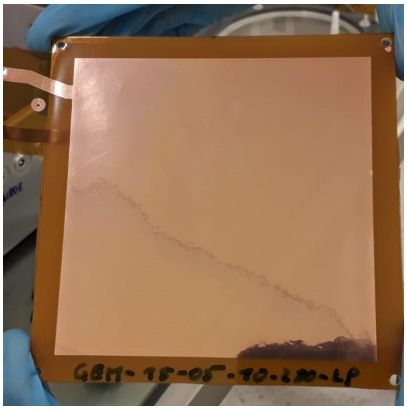

(a) Large Pitch GEM foil.

(b) Bulk Micromegas.

Figure 7: Pictures of GEM and MMG detectors.

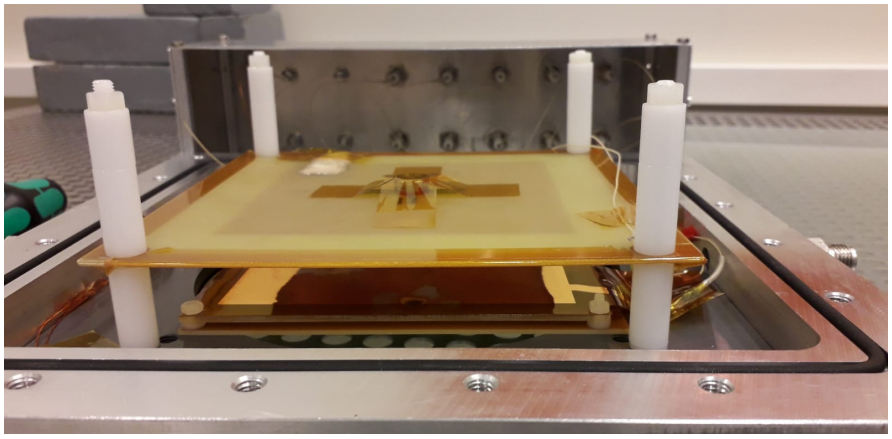

Figure 8: Picture of the hybrid GEM - Micromegas detector.

2.2 Measurements

All the measurements performed followed the same procedure: first the atmospheric pressure, along with the temperature inside and outside the box have been measured. It has also been checked the O_2 and H_2O concentrations in the gas mixture. Traces of O_2 and H_2O can significantly decrease the efficiency of a detector: it is important to maintain high purity of the gas mixture, with contaminant concentrations not higher than ≈ 10 p.p.m. . This is due to the fact that if a gas contains electronegative molecules (such as O_2 or H_2O) electrons can be captured by them, to form negative ions. Capture cross-sections are strongly energy-dependent, and the capture probability is a function of applied field [20]. High values of contamination, leads also to energy resolution degradation.

The currents at the cathode, GEM top and GEM bottom, Micromegas and anode have been measured via picoammeter. Knowing the current values, and using the appropriate equations, gain and IBF have been valuated.
During the measurements, the two detectors have been operated at rather low voltages, and discharges were only rarely observed.

2.2.1 Primary current measurement

Applying only the electric field in the drift region, it is possible to calculate the number of primary electrons created by the ionizing particles coming from the source: E_{drift} only makes the electrons drifting towards the top side of the GEM foil, without causing amplification.
The current consisting of primary electrons, the so called *primary current*, is therefore equal to the current measured on GEM top $I_{\text{GEM}_{\text{top}}}$, when only the drift field is applied: $I_{\text{prim}} = I_{\text{GEM}_{\text{top}}}$. In the case studied here, for the measurement of the primary current, $E_{\text{drift}} = 400$ V/cm. However, it has been observed that the primary current increased during the measurement: since the gain depends on I_{prim}, it is of fundamental importance to determine accurately the value of this current. Due to the fact that the direct measurement was unreliable, a different method has been needed to determine the primary current.

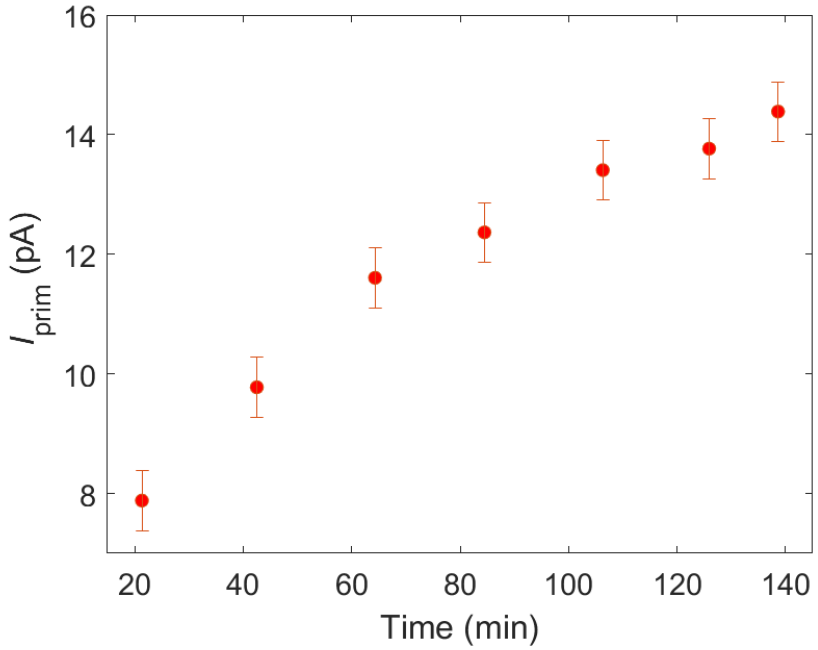

Figure 9: Primary current measured in a time span of about 140 minutes, in the case of ^{55} Fe source.

Knowing the particle rate R and the emitting energy of the source (e.g. for ^{55}Fe), it is possible to evaluate the primary current. Since the average ionization energy of Ar CO_2 90-10 is $E_{\text{i}} = 28.8$ eV, one can determine the number of the electrons ionized by a single photon, which has energy $E_\gamma = 5.9$ keV:

$$I_{\text{prim}} = R \cdot e \cdot \frac{E_\gamma}{E_{\text{i}}}, \tag{4}$$

where e represents the elementary charge.
However, this calculation is only an approximation, because it assumes that each particle emitted by the source generates the same number of electrons when interacting with the gas medium.

2.2.2 Rate measurement

The source rate R represents the number of particles (either α or X-rays) coming from the source into the detector, per unit of time. The value of R, necessary to calculate the primary current using Equation (4), can be obtained computing the integral of the source energy spectrum I_{spectrum}, and dividing the result by the time of measurement t:

$$R = \frac{I_{\text{spectrum}}}{t} \tag{5}$$

I_{spectrum} has been obtained fitting the energy spectrum with the sum of 4 different Gaussian functions: 2 for the main peak, 1 for the escape peak, 1 for the double event peak (for the latter two, see Section 2.2.3).

In the ^{55}Fe case, different spectra have been measured, scanning the transfer field. In Figure 10 it can be noted that the gas gain (proportional to the peak position) increases with the E_{tr}, and tends to reach saturation for $E_{\text{tr}} \approx 700$ V/cm: this indicates that the electrons extraction efficiency of the Standard GEM increases with the transfer field, until it reaches the maximal point.

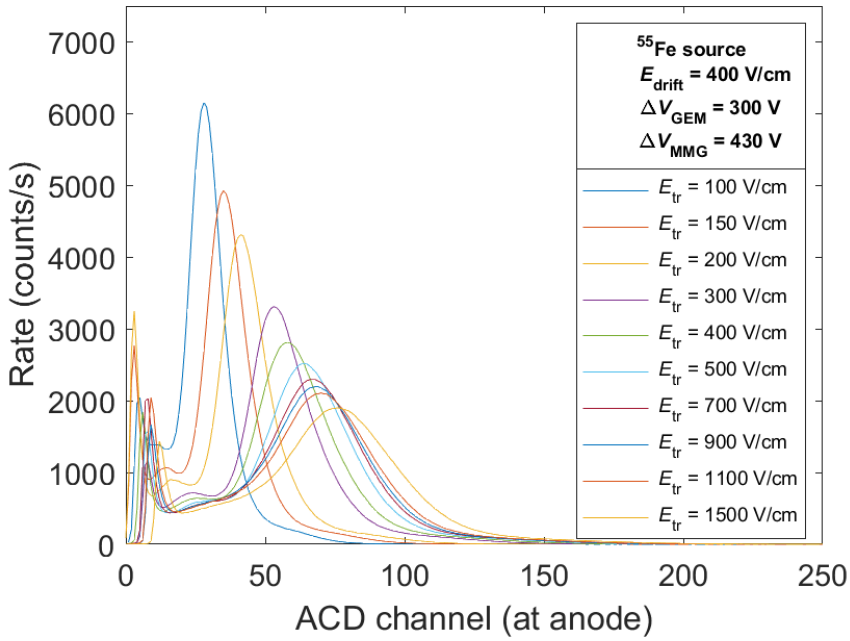

Figure 10: Normalized ^{55}Fe energy spectra, measured scanning E_{tr}.

The rate has been calculated as the average of the integration over the different spectra. It has been found $R = (121 \pm 3)$ kHz, and thus $I_{\text{prim}} = (3.96 \pm 0.09)$ pA. This value has resulted about 10 times more than the one obtained through direct long-time measurements.

Regarding the α source, a rate of (525 ± 5) Hz has been calculated. In this case though, the primary current cannot be evaluated by using Equation (4): as explained in Section 2.1, α particles travel several cm in Ar- CO_2. Since it cannot be concluded that their entire energy is deposited within the active detector volume, the only possible esteem of I_{prim} comes from the direct measurement. For α energy spectrum, which turned to be noisy in most of the cases, see Appendix, Section 8.1.

2.2.3 Energy resolution measurements

The energy resolution has been evaluated from the energy spectrum of ^{55}Fe, fitting with a Gaussian function the main peak. Once the values of the central peak position μ_{peak} and the standard deviation σ_{peak} have been known, E_{res} has been calculated by using Equation (3).

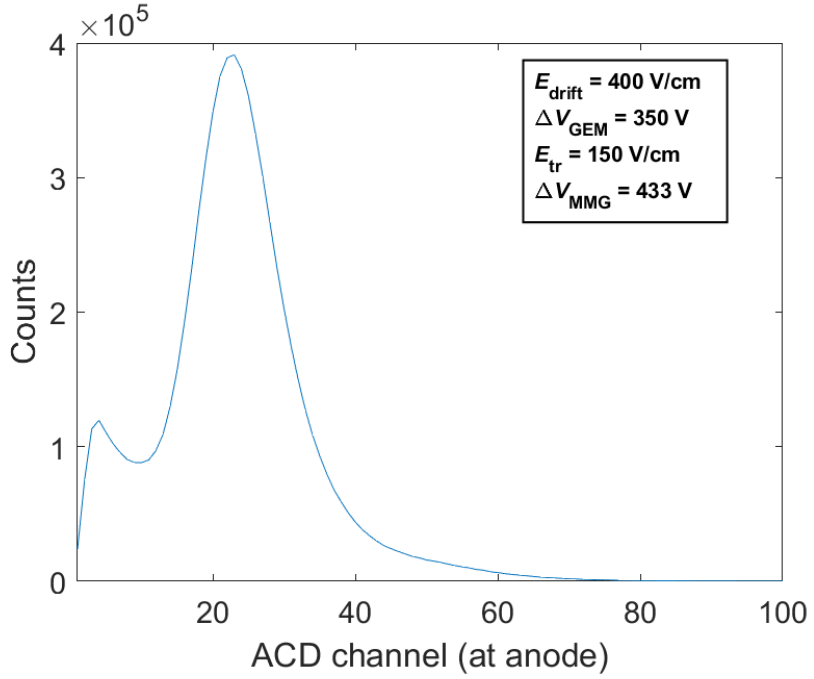

Figure 11: Energy spectrum of ^{55}Fe, measured using the Standard GEM.

As it can be observed in Figure 11, the energy spectrum exhibits two peaks: the *main* peak in the center and the *escape* peak, with less energy.
In the case studied, the photoelectric conversion is the dominant process of interaction between X-rays and matter. If an electron has a binding energy of E_{K} in the K-shell, once ejected from the atom its energy will be: $E = E_\gamma - E_{\text{K}}$, where E_γ is the energy of the ionizing photon (5.9 keV for ^{55}Fe).
The atom the photoelectron belonged to, tends to return to a lower energy state: one electron from the L-shell will disexcite, going to K-shell, and emitting a characteristic X-ray with energy $E'_\gamma = E_{\text{K}} - E_{\text{L}}$. This further photon will be in turn able to ionize other atoms, and to free electrons with energy $E_{\text{escape}} = E'_\gamma - E_{\text{K}}$, which will form the escape peak.
According to the theory, the energy spectrum can exhibit a further peak, the so called *double event* peak. This peak, caused by two source particles arriving in the detector at approximately the same time, is located in the rightmost part of the spectrum. Since its amplitude is usually very low, in the spectra analyzed it turned to be hard to distinguish it.

2.2.4 Oscilloscope signals

When energy resolution measurements are performed, the detector noise has to be kept as low as possible. In order to monitor the noise, during energy resolution measurements, the anode has been connected, through a preamlifier and an amplifier, to

an oscilloscope, which displayed the signal, consisting of the entire electron cloud approaching to the anode.
The signal noise has been sensibly dimineshed by shielding the detector cables and the preamplifier with copper wires.

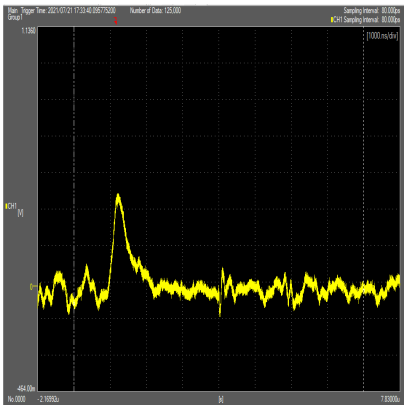

(a) Gain 8890.

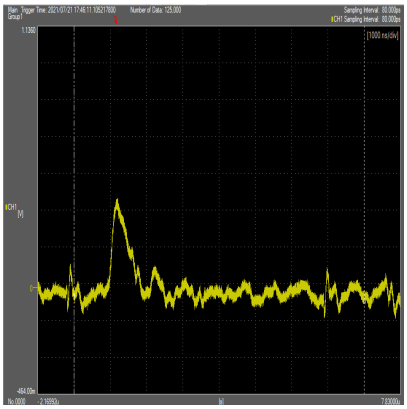

(b) Gain 9130.

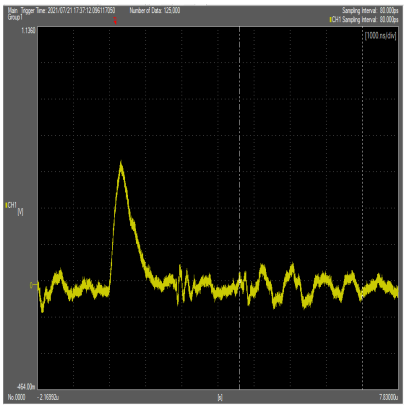

(c) Gain 13600.

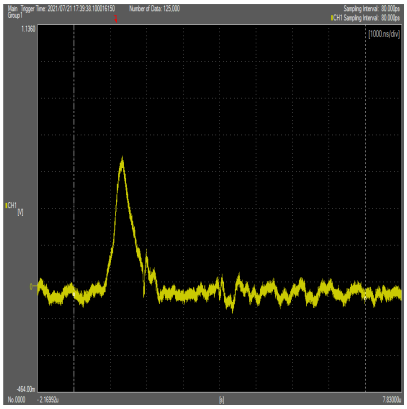

(d) Gain 18000.

Figure 12: ^{55}Fe signals displayed by the oscilloscope.

In the case depicted here, $E_{\text{drift}} = 400$ V/cm, $\Delta V_{\text{GEM}} = 400$ V, $E_{\text{tr}} = 150$ V/cm, and ΔV_{MMG} varies from 371 to 428 V.
As expected, the signal results higher when the gain increases: with more amplification, more electrons are created, thus increasing the signal detected.

3 Measurements of currents

In order to characterize the detector, currents induced on all electrodes have been measured: the scans performed in this stage of the experiment have been later used to evaluate gain and IBF values. In all cases, the algebraic sum of the currents has resulted sensibly close to zero, in accordance with the charge conservation. The signal induced on the readout anode is caused by the amplified electrons, while the drift cathode current is due to backdrifting ions, from amplification stages to the drift region.

3.1 Currents scanning ΔV_{MMG}

Measurements were firstly performed scanning ΔV_{MMG}, while keeping the other parameters constant.

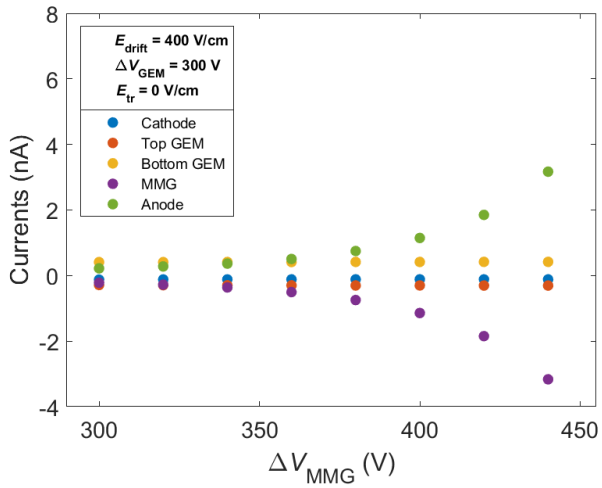

(a) E_{tr} = 0 V/cm.

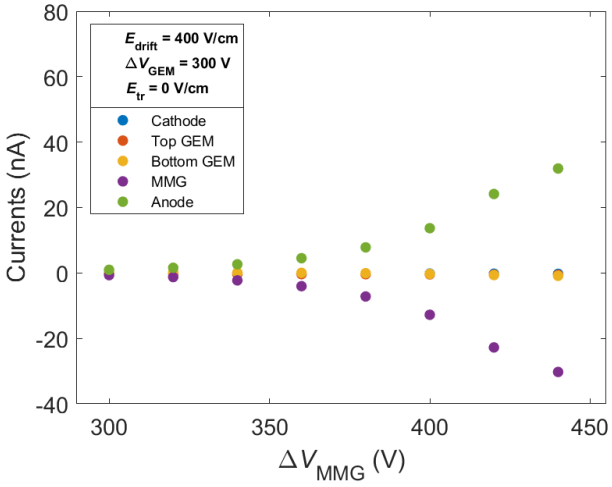

(b) E_{tr} = 4000 V/cm.

Figure 13: Currents measured scanning ΔV_{MMG}, for different values of E_{tr}. Error bars are within the dimension of experimental points.

For $\Delta V_{\mathrm{MMG}} < 350$ V, the currents are approximately equal for each stage (Figure 13): in this configuration the amplification is therefore very low. Whit increasing ΔV_{MMG}, Micromegas and anode currents get higher (about 2 orders of magnitudes more than the other electrodes), due to the charge amplification. Signals on these electrodes are induced by both electrons and ions, drifting within the amplification gap in opposite directions. The opposite direction of the charges, cause thus the opposite polarity of Micromegas and anode.
Moreover, a dependence on the transfer field can be observed on Panels (a) and (b) of Figure 13: the maximum current reached with $E_{\mathrm{tr}} = 0$ V/cm, is only 4 nA, while for $E_{\mathrm{tr}} = 4000$ V/cm, $I_{\mathrm{anode}} = 40$ nA can be easily attained.

3.2 Currents scanning E_{tr}

To further study the dependence of the currents on E_{tr}, a scan of the transfer field has been performed, shown in Figure 14.

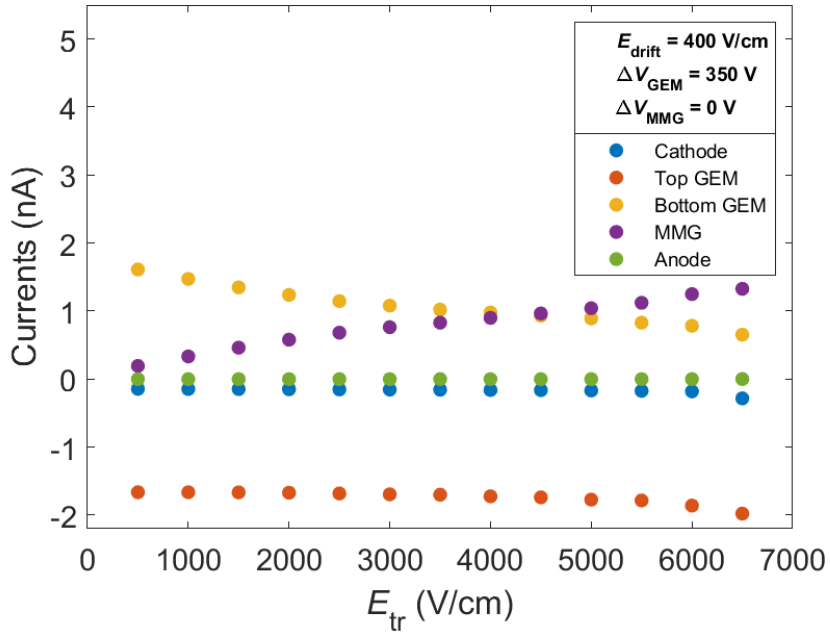

Figure 14: Currents measured scanning E_{tr}.
Error bars are within the dimension of experimental points.

For low values of E_{tr}, GEM bottom current $I_{\mathrm{GEM_{bottom}}}$, is higher than Micromegas current, I_{MMG}. For high fields, on the contrary, $I_{\mathrm{GEM_{bottom}}} < I_{\mathrm{MMG}}$. After the avalanche inside GEM holes, for low E_{tr}, most of the electrons are not extracted towards the Micromegas stage, terminating at the bottom part of the GEM. When E_{tr} increases, on the other hand, the GEM extraction efficiency is larger, and more electrons reach the MMG mesh.
In this example the anode current is close to zero, because no amplification occurs at the Micromegas stage.

Current measurements scanning ΔV_{GEM} have been also performed, finding a similar trend as in ΔV_{MMG} scan case (see Appendix 8.2).

4 Gain studies

Once the current induced at the anode stage I_{anode} has been measured, and the primary current I_{prim} has been calculated using Equation (4), it is possible to evaluate the detector effective gain G:

$$G = \frac{I_{\text{anode}}}{I_{\text{prim}}} \tag{6}$$

As expected from previous studies [21], it has been found that G increases exponentially with the applied voltage, either ΔV_{GEM}, or ΔV_{MMG}. Keeping the detector gain, E_{drift} and E_{tr} constant (the latter equal or greater than 150 V/cm), it has been observed that if ΔV_{GEM} decreases, ΔV_{MMG} needs to be increased. Their sum is not constant though: as ΔV_{GEM} gets smaller, the sum $\Delta V_{\text{GEM}} + \Delta V_{\text{MMG}}$ has to be increased, in order to obtain a constant G (for example, see Tables 3 and 5 on Appendix). This result confirms that Micromegas provides most of the hybrid detector gain.
Previous researches [21] proved that in the case of a GEM - GEM detector, the voltage is evenly distributed between the two foils, and the sum remains constant, for 600 V $< \Delta V_{\text{GEM}_1} + \Delta V_{\text{GEM}_2} <$ 900 V, E_{drift} = 3 kV/cm, E_{tr} = 4.4 kV/cm.
Gain studies have been performed with α source, and if not otherwise precised, using the Standard GEM.

4.1 Gain as a function of ΔV_{MMG}

The effective gain has been then studied for different values of E_{tr}, scanning the Micromegas voltage, while keeping E_{drift} = 400 V/cm and ΔV_{GEM} = 300 V.

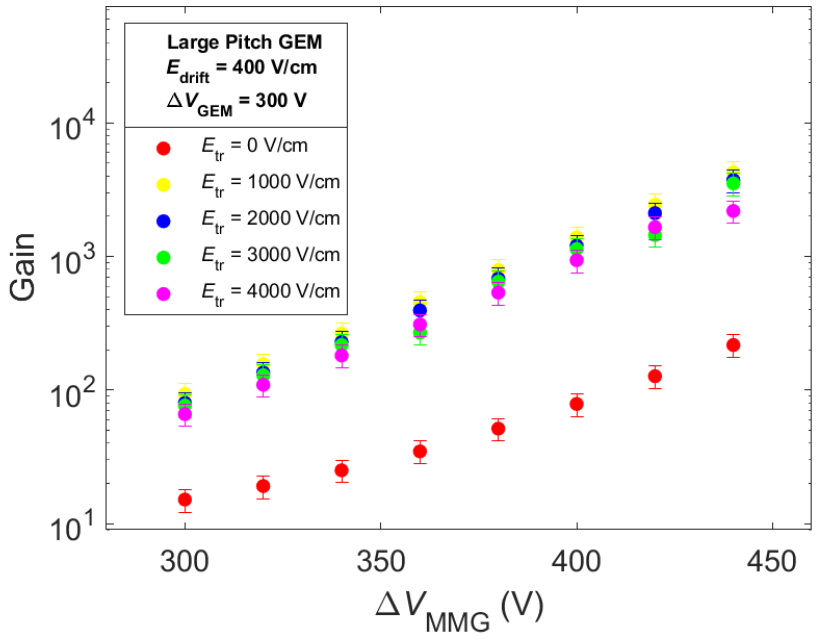

Figure 15: Gain as a function of ΔV_{MMG}, for different value of the transfer field.

As already explained in Section 2.2.2, the effective gain increases for higher values of the transfer field until saturation, which indicates the maximum point of electron transfer efficiency [15] in the GEM. As it can be observed in Figure 15, the saturation point is achieved for $E_{\text{tr}} \leq$ 1000 V/cm: from that value on, the gain does not increase

with the transfer field, resulting on the contrary slightly less for higher values of E_{tr}. In E_{tr} = 0 V/cm case, once electrons pass through the GEM, they do not get accelerated towards the Micromegas, but rather, following the fields lines, they reach GEM bottom stage. Every ion-electron pair created in the transfer region recombines, without causing any signal. The current measured at the anode stage is mostly caused by the electrons formed within the Micromegas amplification gap, which get amplified by MMG mesh only.

The same scans here described have been performed applying a voltage ΔV_{GEM} = 350 V, and comparing this result with ΔV_{GEM} = 300 V case (see Appendix, Section 8.3). Even when E_{tr} = 0 V/cm, the gain is less for ΔV_{GEM} = 300 V case: GEM stage thus plays a role on the detector gain, even when there is no electric field in the transfer region.

4.1.1 Single Micromegas and hybrid detector

The effective gain of hybrid GEM - Micromegas detector has been compared with single Micromegas gain, previously obtained with a similar setup, and a drift gap of 20 mm [22].

For both cases, E_{drift} = 400 V/cm, while for GEM - Micromegas case, ΔV_{GEM} = 350 V, and E_{tr} = 1000 V/cm.

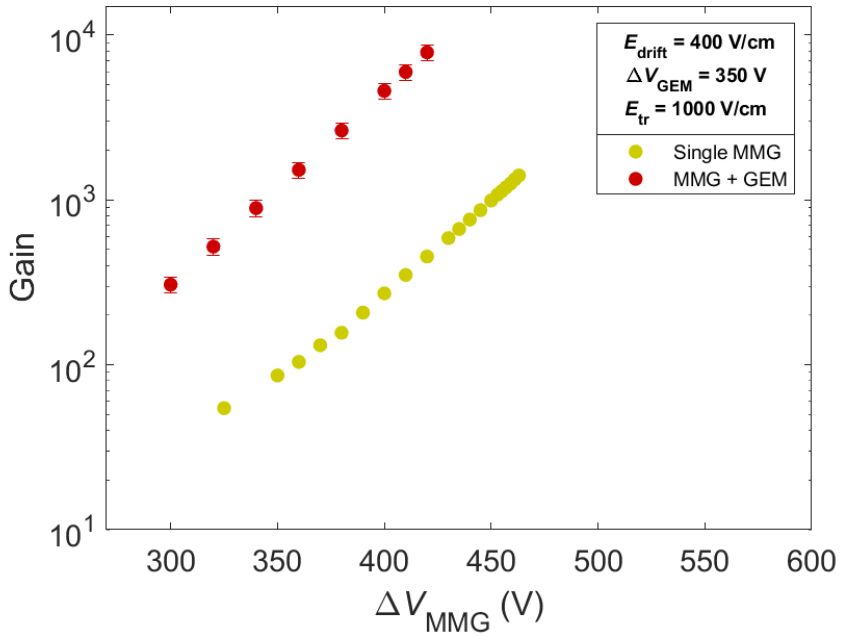

Figure 16: Comparison between single MMG and GEM - MMG gains. When not visible, error bars are within the dimension of experimental points.

In the hybrid detector, the GEM foil works as a preamplifier stage, accelerating and amplifying electrons towards the Micromegas mesh. Therefore, as expected, the effective gain has resulted about 10 times more for the Micromegas - GEM setup rather than for the single MMG (Figure 16).

4.2 Standard and Large Pitch GEM

The detector gain measured with the Standard, and with the Large Pitch GEM have been compared. The Micromegas mesh is the same for both setup: it is thus possible to compare the gas gains at GEM stage, calculated as:

$$G_{\mathrm{GEM}} = \frac{I_{\mathrm{GEM_{bottom}}}}{I_{\mathrm{prim}}}, \tag{7}$$

when $E_{\mathrm{drift}} = 400$ V/cm, $E_{\mathrm{tr}} = 0$ V/cm and $\Delta V_{\mathrm{MMG}} = 0$ V.

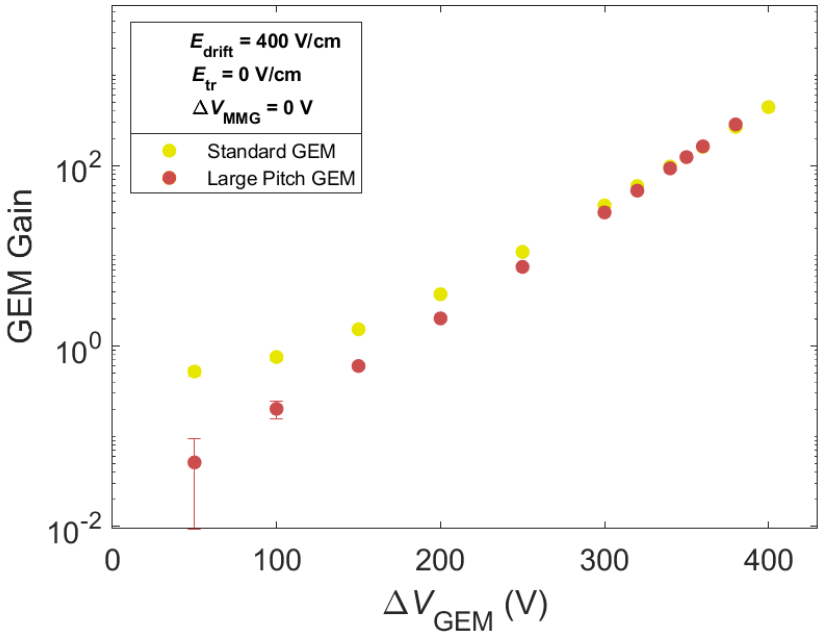

Figure 17: Comparison between Standard and Large Pitch GEM gains.
When not visible, error bars are within the dimension of experimental points.

In Figure 17 Large Pitch gain increases exponentially with ΔV_{GEM}, as expected. In Standard GEM case, however, for low values of the voltage, a initial flex can be observed.
For $\Delta V_{\mathrm{GEM}} < 200$ V, $G_{\mathrm{GEM}} < 1$, meaning that the electrons which induce a signal at the top GEM stage are more than the electrons at the bottom. This result could be caused either by the positive ions, which from the transfer region hit bottom GEM, and neutralize the negative charges, or by the rather low extraction efficiency values. In any case, the voltage range for which $G_{\mathrm{GEM}} < 1$, does not represent the region the detector is aimed to be operated.

In the first part of the scans, the Standard GEM foil exhibits higher gain than the Large Pitch foil. This behaviour is due to the two foils collection efficiency, ϵ_c^-. It can be shown that $G \propto \epsilon_c^-$ [23]: since for low values of ΔV_{GEM}, Standard GEM collection efficiency is better than Large Pitch's one [24], the former achieves higher gains. In correspondence of the gain meeting point, for both GEMs $\epsilon_c^- \approx 100\%$.

5 Ion backflow studies

Referring to Equation (2), ion backflow has been calculated as the ratio of cathode to anode current. Moreover, the effective gain plays a fundamental role on IBF studies: as already explained in Section 1.1, $IBF \cdot G = (\epsilon + 1)$, where ϵ is the number of ions drifting back to the drift volume, per incoming electron from the amplification regions. Knowing ϵ, it is possible to compare different setups and gas mixtures.
Ion backflow also includes a contribution from ions created during the primary ionization process.
If not otherwise specified, these studies have been performed using α source, and the Standard GEM.

5.1 Ion backflow as a function of E_{drift}

One of the most important parameters that characterizes the ions feedback is the electric field applied in the drift volume. As a matter of fact, increasing E_{drift}, ions formed from GEM top electrode have a higher probability to escape to the drift volume.
The optimum value of the E_{drift} is reached when it is strong enough to create primary electrons with sufficient drift velocity to push them through GEM holes, but also small enough to keep IBF low.

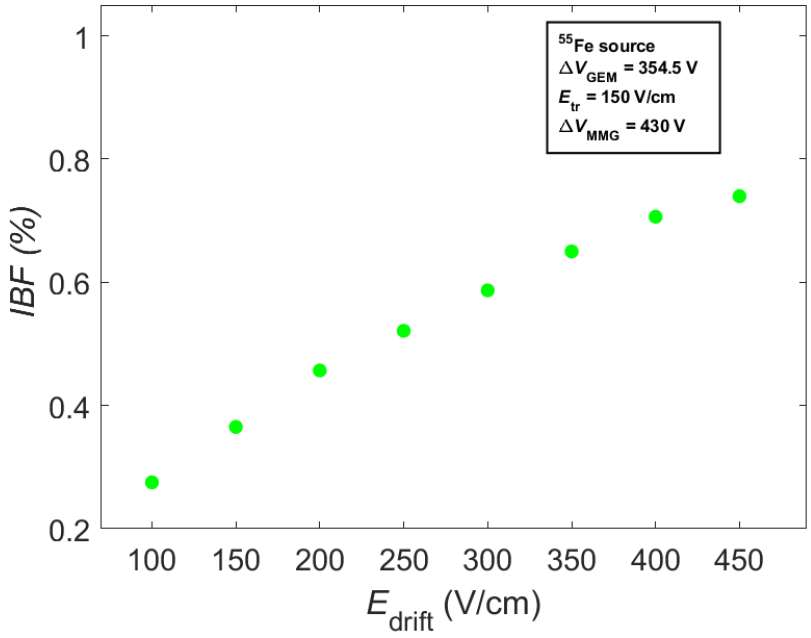

Figure 18: ion backflow as a function of E_{drift}.
Error bars are within the dimension of experimental points.

Shown in Figure 18, IBF depends linearly on E_{drift}, with a linear coefficient of determination $R^2 = 0.986$.

5.2 Ion backflow as a function of E_{tr}

The ion backflow has been studied scanning E_{tr}, tuning either GEM or Micromegas voltage, to obtain a constant effective gain. E_{drift} has been kept 400 V/cm during all

the study. Increasing E_{tr} throughout the scan, the adjusted GEM (Micromegas) voltage has been gradually diminished, in order to keep G fixed. When E_{tr} = 600 V/cm, a different behaviour has been observed: ΔV_{GEM} (ΔV_{MMG}) had to be kept constant for higher values of the transfer field, indicating that the maximum point of GEM extraction efficiency ϵ_e^- was reached. A similar behaviour has been observed for the Large Pitch GEM: in this case though, the turning point was represented by E_{tr} = 400 V/cm, and from this value on, the adjusted voltage needed to be increased, rather than kept fixed. The maximum ϵ_e^- in LP case is achieved for lower E_{tr}, due to the GEM *optical transparency*: this quantity, defined as the ratio of the open to the total area of a foil, is more for Standard than Large Pitch GEM. Since ϵ_e^- depends inversely on the optical transparency [24], its maximum value is reached more easily using LP GEM.

5.2.1 ΔV_{GEM} adjusted

As it can be observed in Figure 19, when ΔV_{GEM} is adjusted, *IBF* decreases with E_{tr}, up to a minimum (of about 100 ÷ 200 V/cm, depending on the Micromegas voltage). For low values of the transfer field, ΔV_{GEM} is large: since with this configuration ions escape more easily from the GEM, *IBF* reaches high values. Increasing E_{tr} the extraction efficiency gets higher: the GEM can therefore operate at lower voltages. After the minimum is reached, *IBF* starts to slowly increase with the transfer field: for higher values of E_{tr}, more ions are extracted from Micromegas stage. The minimum point, though, does not correspond to the minimum value of ΔV_{GEM}, which is reached for E_{tr} = 400 V/cm (further details on Table 1).

The ion feedback has resulted less for higher ΔV_{MMG}: the ion production in the MMG stage is compensated by the increased ion capture, due to the increase in the ratio of E_{ampl} to E_{tr}. For a study of *IBF* as a function of ΔV_{MMG}, see Appendix 8.5.

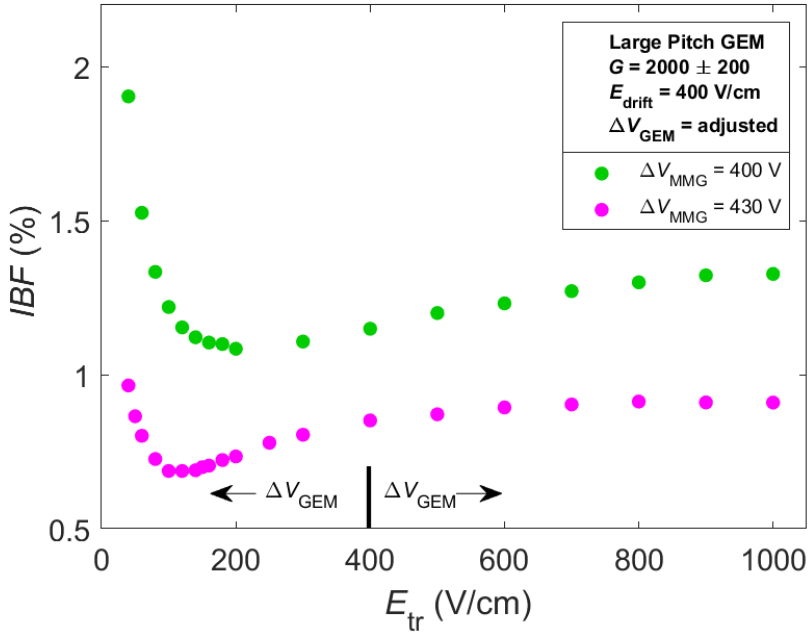

Figure 19: ion backflow as a function of E_{tr}, tuning ΔV_{GEM}.
Error bars are within the dimension of experimental points.

5.2.2 ΔV_{MMG} adjusted

In ΔV_{MMG} tuning case, IBF increases with E_{tr}, until saturation, for E_{tr} = 400 V/cm. After the saturation, the ion backflow slightly decreases, in correspondence of ΔV_{MMG} increase (Figure 20). It has been observed that IBF is more pronounced for higher ΔV_{GEM}: increasing the voltage, the charge amplification is higher, and thus more ions are created at GEM stage. IBF as a function of ΔV_{GEM} is studied in detail in Section 8.5 of the Appendix.

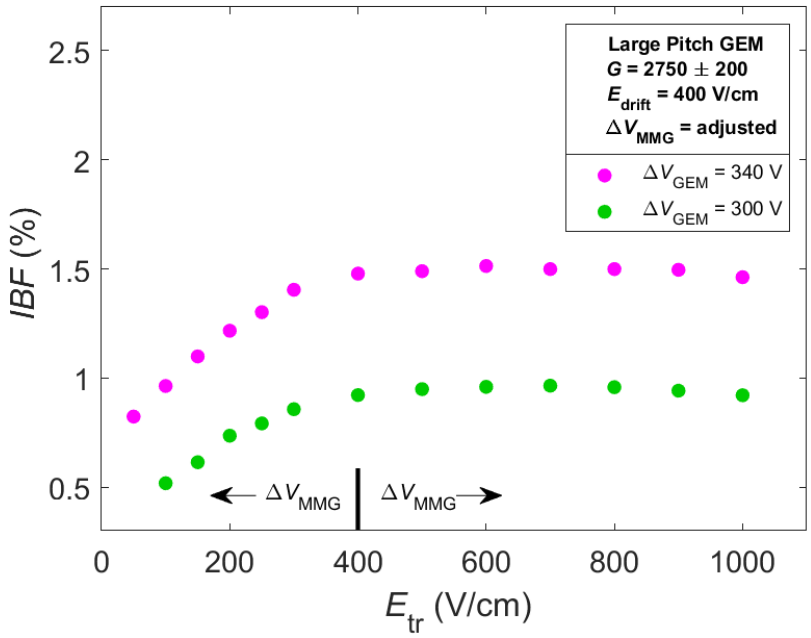

Figure 20: ion backflow as a function of E_{tr}, tuning ΔV_{MMG}.
Error bars are within the dimension of experimental points.

Ion backflow values are listed in the following tables. As it can be observed, the adjusted voltage (either ΔV_{GEM} or ΔV_{MMG}) reaches a minimum when E_{tr} = 400 V/cm.

E_{tr} (V/cm) (±1 V)	ΔV_{GEM} (V) (±1 V)	IBF(%) (±4 · 10^{-4})
100	340	1.176
200	315	1.068
400	305	1.149
600	310	1.232
800	315	1.300
1000	320	1.327

(a) ΔV_{GEM} adjusted, ΔV_{MMG} = 400 V.

E_{tr} (V/cm) (±1 V)	ΔV_{MMG} (V) (±1 V)	IBF(%) (±4 · 10^{-4})
100	450	0.518
200	430	0.735
400	421	0.922
600	426	0.959
800	429	0.958
1000	433	0.921

(b) ΔV_{MMG} adjusted, ΔV_{GEM} = 300 V.

Table 1: ion backflow values, scanning E_{tr} with LP GEM, for E_{drift} = 400 V/cm.

5.2.3 Standard and Large Pitch GEM

The ion backflow has been studied comparing Standard and Large Pitch GEM behaviour. As depicted in Figure 21, the *IBF* trend results the same for both cases, reaching a minimum when $E_{tr} \approx 200$ V/cm.

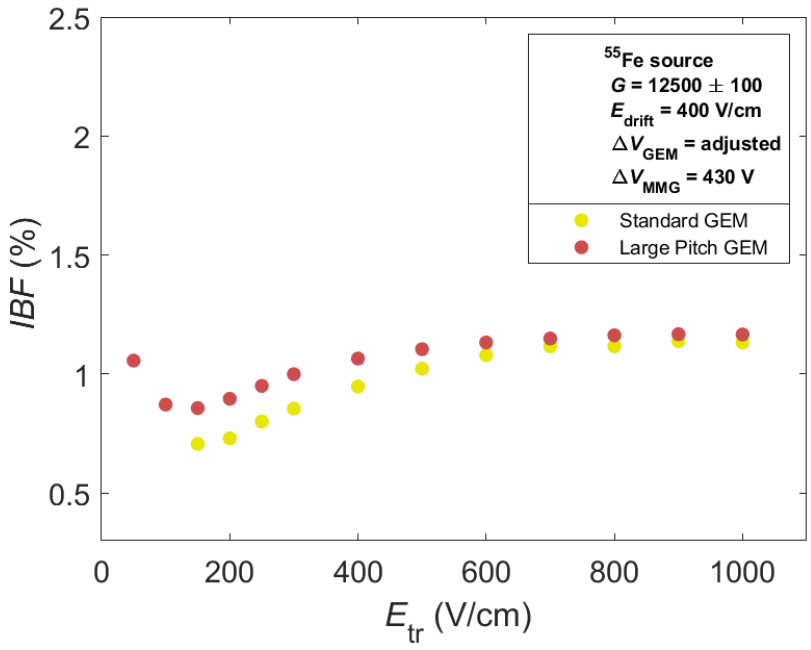

Figure 21: ion backflow as a function of E_{tr}.
Error bars are within the dimension of experimental points.

In order to reach the same gain, ΔV_{GEM} needs to be higher for Standard GEM (Table 2), confirming that the extraction efficiency in this case is worse than for LP foil. On the other hand, *IBF* results are a convolution of several effects: since it both depends on extraction and collection efficiency, and on the optical transparency, further studies are required to fully understand its behaviour.

E_{tr} (V/cm) (± 1 V)	ΔV_{GEM} (V) (± 0.1 V)	$IBF(\%)$ ($\pm 1 \cdot 10^{-4}$)
200	375.0	0.730
400	361.5	0.948
600	358.2	1.079
800	358.2	1.116
1000	358.5	1.132

(a) Gain = 12500, Standard GEM.

E_{tr} (V/cm) (± 1 V)	ΔV_{GEM} (V) (± 0.1 V)	$IBF(\%)$ ($\pm 4 \cdot 10^{-4}$)
200	342.0	0.896
400	328.5	1.065
600	332.0	1.133
800	337.0	1.163
1000	341.0	1.166

(b) Gain = 12500, Large Pitch GEM.

Table 2: ion backflow values, scanning E_{tr} with Standard and Large Pitch GEM, for $E_{drift} = 400$ V/cm, $\Delta V_{MMG} = 430$ V.

6 Energy resolution studies

The principal parameters related to detectors performances are energy resolution and ion backflow: in order to optimize the device, a study of the functional relation between these two quantities is therefore of great importance. Direct measurements and simulations exhibit a characteristic anti-correlation between ion backflow and the relative energy resolution [25]. While the ions created at the MMG stage can be blocked by the upper GEM layer, the ions from GEM have a large probability to escape into the drift volume. The number of ions produced by GEM can be decreased reducing the amplification: this leads however to larger GEM gain fluctuations with consequent degradation of the energy resolution. The goal is then to find an operational region with the required detector performances (described in Section 1.4), by tuning voltages and fields. Better energy resolution requires in general higher gains provided by the GEM, while *IBF* favour lower GEM's gains [26]. Since both ion feedback and energy resolution are functions of the gain, measurements were performed keeping G constant. Hence, for this study, one of the 4 variables has been scanned, another one was adjusted to keep the gain constant, and the other two were kept fixed.
Energy resolution errors may seem quite high, due to the large 10×10 cm^2 pad to readout signals used. However, the main goal of this experiment is the study of trends and functional dependences, rather than detailed absolute numbers.

6.1 ΔV_{GEM} scans

In this Section, the behaviour of energy resolution as a function of ion backflow has been studied for 4 different values of gain, scanning ΔV_{GEM} from 330 V to 400 V. In order to keep G constant for each set, the Micromegas voltage has been adjusted, whereas E_{tr} = 150 V/cm and E_{drift} = 400 V/cm. For the same value of ΔV_{GEM}, higher gains have been achieved by increasing the adjusted ΔV_{MMG}.

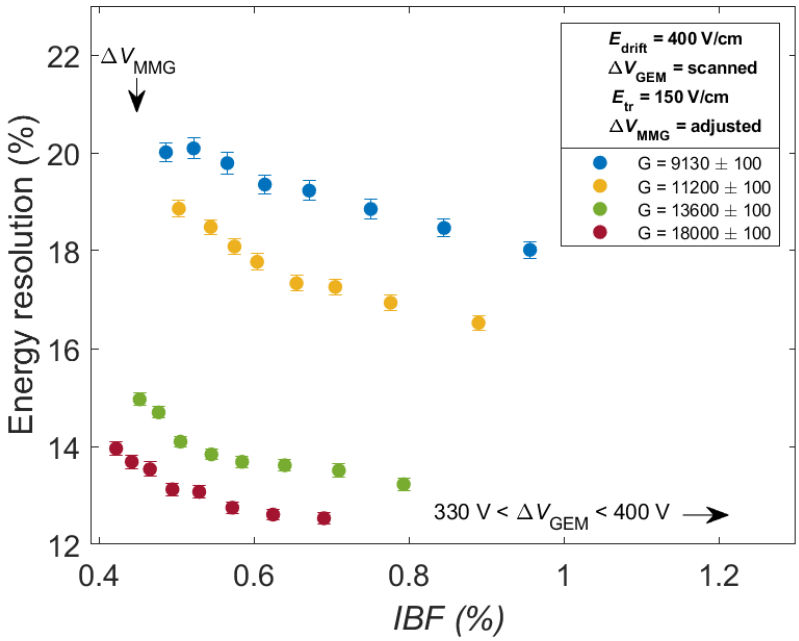

Figure 22: energy resolution as a function of ion backflow, for ΔV_{GEM} scans.

As predicted, Figure 22 shows that good energy resolution corresponds to large ion backflow, and vice versa. The *IBF* is less than 1% for every value of ΔV_{GEM} scanned. Gains of 9130 and 11200 don't meet Hydra requirements, since the energy resolution results 16% at the least.
As it can be observed in Figure 22, higher gains correspond to better energy resolution and lower *IBF*. This behaviour can be explained as it follows: since E_{tr} and E_{drift} are constant, in order to increase the gain, ΔV_{MMG} value has to be higher. Higher voltages at MMG stage, mean more electrons production, and thus better energy resolution. Moreover, as already shown in Section 5.2.1, *IBF* decreases with ΔV_{MMG}, when the other parameters are fixed.

6.1.1 Standard and Large Pitch GEM

The same measurements performed with Standard GEM have been repeated using the Large Pitch GEM. The relation between energy resolution and *IBF* is once again in accordance with the predictions.
For the same values of gain and ΔV_{GEM}, the adjusted ΔV_{MMG} has resulted lower for the Large Pitch case, due once again to the higher extraction efficiency.

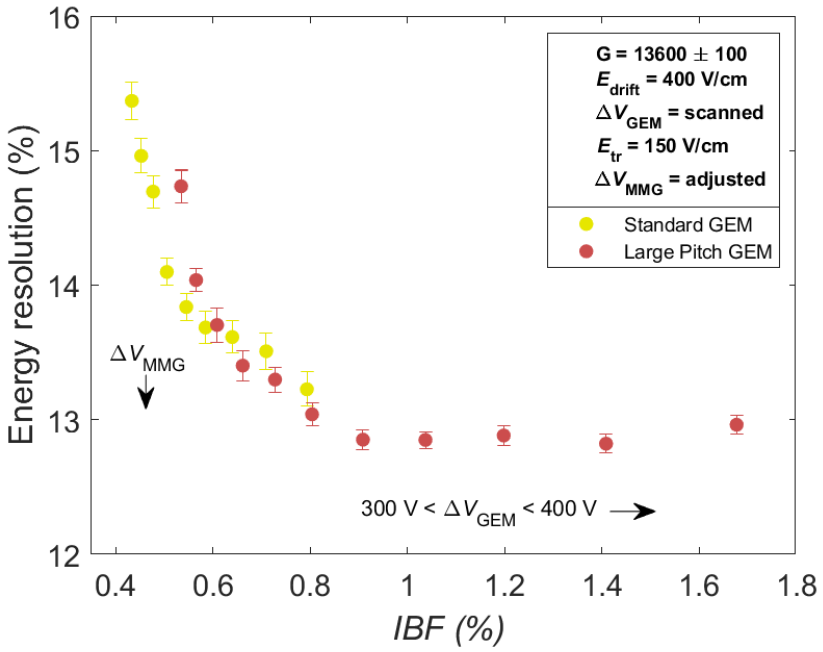

Figure 23: energy resolution as a function of ion backflow, for ΔV_{GEM} scans. Comparison between Standard and Large Pitch GEM.

Comparing the two trends depicted in Figure 23, it can be concluded that Large Pitch GEM is characterized by worse energy resolution. This result is caused by the two foils collection efficiency: it can be shown that $E_{\text{res}} \propto 1/\sqrt{N^-}$, where N^- represent the number of electrons collected by the detector, depending on ϵ_c^- [23]. Since ϵ_c^- is higher for Standard GEM, its energy resolution will subsequently be better than Large Pitch's. The meeting point of the two plots, represents the point where the collection efficiency of both GEMs reaches 100%. For further details on energy resolution and *IBF* values refer to Section 8.6.1, Tables 4 and 5.

6.2 E_{drift} scans

Next, the drift field has been scanned, from 100 to 500 V/cm. While E_{tr} = 150 V/cm and ΔV_{MMG} = 430 V, the voltage applied between GEM top and GEM bottom, ΔV_{GEM}, has been adjusted.
Accordingly to the expectations [26], it has been found that the gain changes very weakly with E_{drift}: in order to keep G constant, ΔV_{GEM} has been changed at most of only 2 V.
An effective gain of 12700 ± 100 corresponds to ΔV_{GEM} = (384 ± 2) V, while for G = 21100 ± 100, the voltage applied was ΔV_{GEM} = (406 ± 2) V.
Once more, energy resolution increases when ion backflow decreases, and higher gains correspond to better energy resolution (shown in Figure 24).

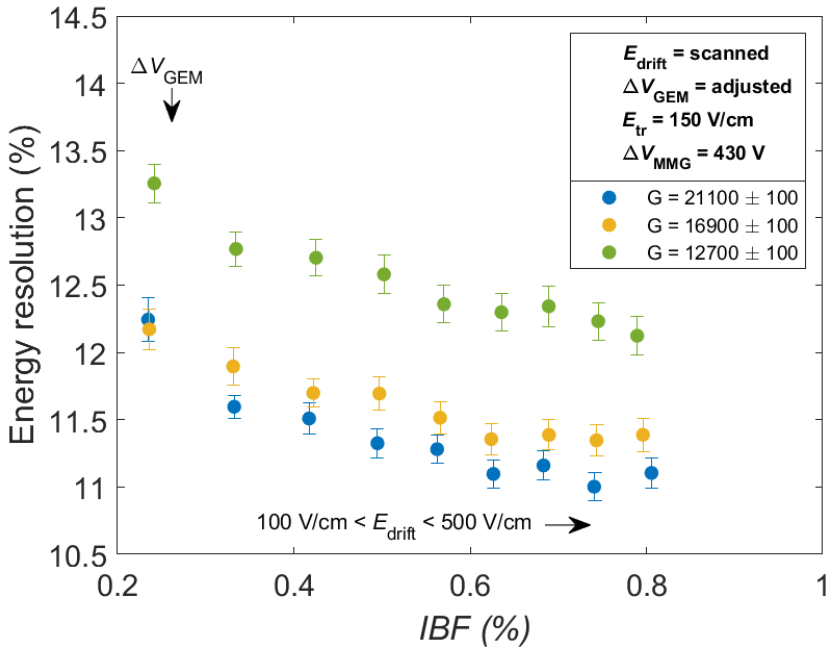

Figure 24: energy resolution as a function of ion backflow, for E_{drift} scans.

In this case the energy resolution depends only on ΔV_{GEM} because the other parameters are constant, or don't influence it. Higher voltages on GEM implies better energy resolution: therefore, these results confirm the expectations.
The total range studied exhibits $IBF < 1\%$, and energy resolution $< 15\%$, in accordance with the requirements needed. The values of energy resolution and of ion backflow are listed in the Appendix, 8.6.2.

Also in this case, the scans have been performed with both the Standard and the Large Pitch GEM, and, once again, the energy resolution has resulted worse for LP. Since E_{drift} is increased, probably the collection efficiency does not reach 100%.
For more details, see Figure 33 in Appendix Section.

6.3 E_{tr} scans

The field applied between GEM and Micromegas detectors has been scanned from 150 V/cm to 1000 V/cm, adjusting ΔV_{GEM}, while keeping E_{drift} = 400 V/cm, and ΔV_{MMG} = 430 V.

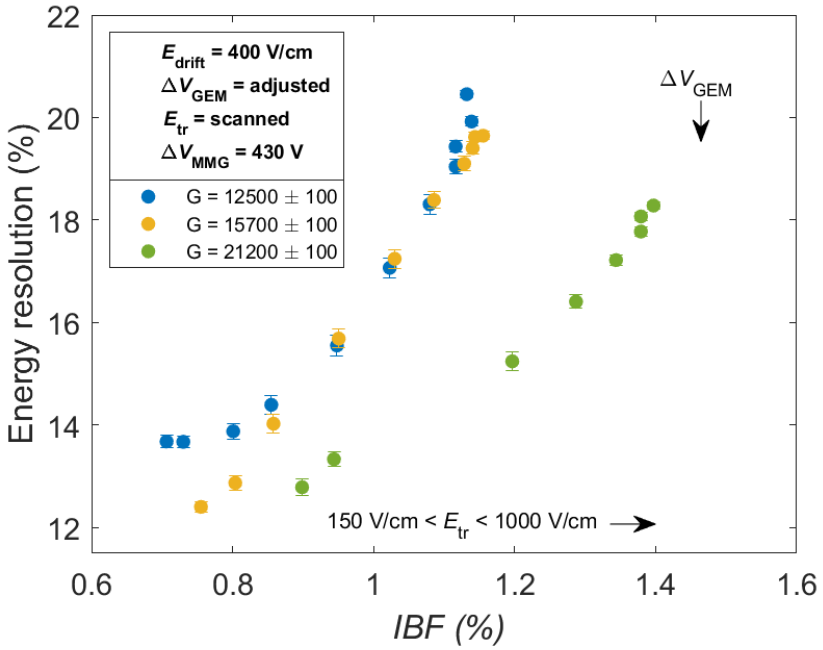

Figure 25: energy resolution as a function of ion backflow, for E_{tr} scans. When not visible, error bars are within the dimension of experimental points.

On the contrary of the precedent studies, Figure 25 shows that in this case the energy resolution increases with the ion feedback.
It has been already demonstrated that, for $E_{tr} \geq 200$ V/cm, the *IBF* increases with the transfer field, when ΔV_{GEM} is adjusted (Section 5.2.1). When E_{tr} increases, the effective gain of the GEM increases, due to enhanced electron extraction efficiency, and thus improving the energy resolution. At the same time, in order to keep the gain constant, ΔV_{GEM} needs to be decreased as E_{tr} gets larger: this cause the effective gain of GEM to decrease, which in turn degrades the energy resolution. The results in Figure 25 demonstrate that the two effects do not compensate each other, but that the degradation of energy resolution, caused by smaller ΔV_{GEM} values, prevails over the E_{res} improvement due to larger E_{tr}. In any case, this conclusion can be only drawn for the range of voltages and electric fields studied. More details on their values can be found in Section 8.6.3.
Moreover, it has been observed that, for $E_{tr} \geq 600$ V/cm, an increase of the transfer field does not affect the gain, which remains constant (the same result has been found with α source, and presented in Section 5.2). The GEM electron extraction efficiency reaches the maximum, and, since ΔV_{GEM} is not tuned anymore, *IBF* and E_{res} change only slightly.
For most of the range studied, especially for high values of the transfer field, $IBF > 1\%$ and $E_{res} > 15\%$, not fitting the parameters needed. In order to meet the requirements, E_{tr} has to be kept lower than 350 V/cm.

6.3.1 Standard and Large Pitch GEM

Comparison between the two GEMs behaviour has been once again made.
The results in Figure 26 show that for Large Pitch case, not only the energy resolution does not decrease with ion feedback, but also the E_{res} does not follow any specific trend. Furthermore, in the range of parameters scanned, for the same value of IBF the energy resolution results better for the LP GEM rather than the Standard one, at odds with the previous results and the predictions.

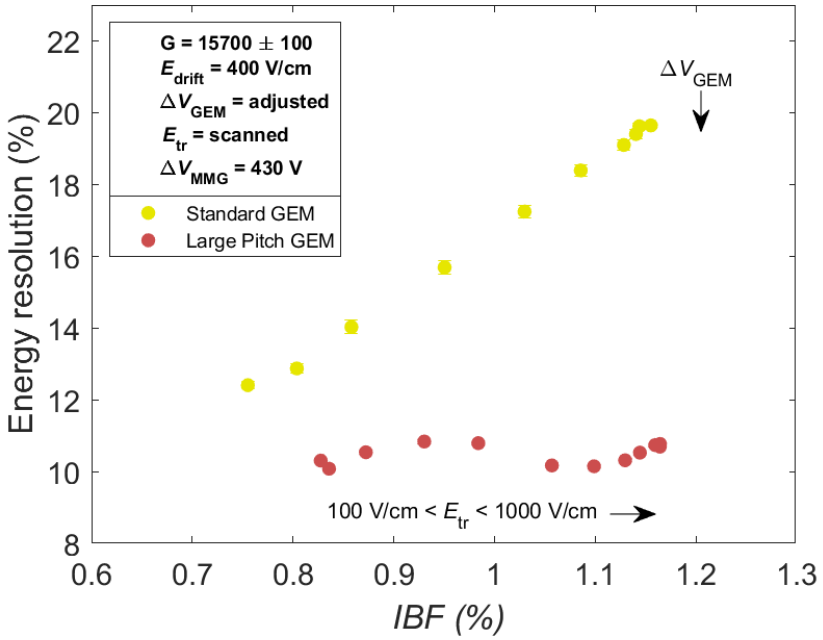

Figure 26: energy resolution as a function of ion backflow, for E_{tr} scans.
Comparison between Standard and Large Pitch GEM.
Error bars are within the dimension of experimental points.

For Large Pitch GEM, the relation between the energy resolution and the ion backflow has resulted the same for all the gains studied (see Section 8.6.3, Figure 34). Since any satisfying explanation have not been found yet, further investigations will be certainly performed in the future.

6.4 E_{tr} scans - ΔV_{MMG} adjusted

The same scans with the transfer field have been performed by adjusting the voltage between the Micromegas and the anode, while keeping E_{drift} = 400 V/cm, and ΔV_{GEM} = 370 V.
As it can be observed in Figure 27, the energy resolution firstly decreases with ion backflow, until it reaches a minimum. For both gains the minimum point is reached when $IBF \approx 0.75\%$ and $E_{res} \approx 12\%$. This values correspond to E_{tr} = 250 V/cm, and to ΔV_{MMG} = 430 V for gain 12500, while ΔV_{MMG} = 440 V for G = 15700. After the minimum, the energy resolution increases with IBF.
According to the results of Section 5.2.2, it has been found that the ion backflow increased with E_{tr} until the saturation point of 600 V/cm.

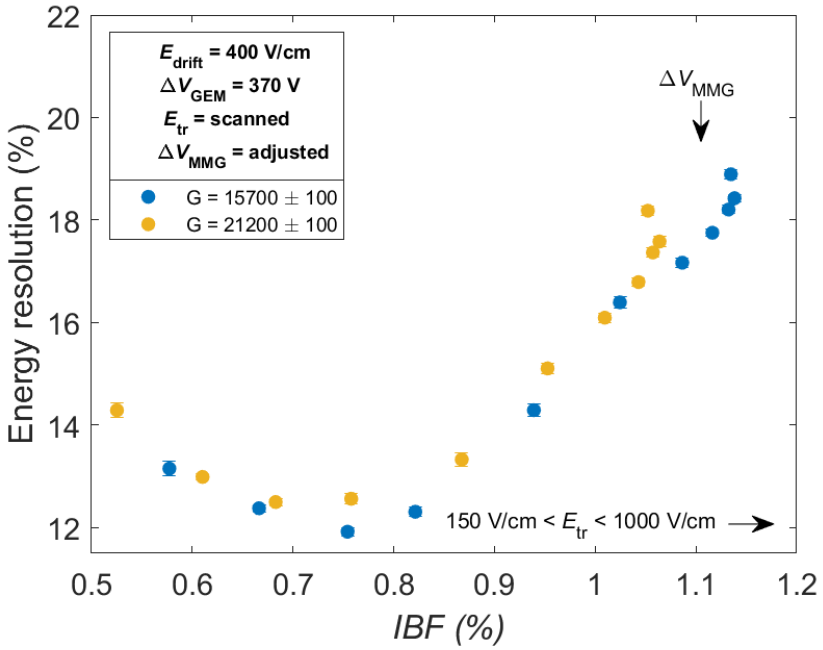

Figure 27: energy resolution as a function of ion backflow, for E_{tr} scans adjusting ΔV_{MMG}.
When not visible, error bars are within the dimension of experimental points.

The energy resolution improves when the transfer field is large, but it degrades if the Micromegas voltage decreases. It is therefore possible that for low values of the transfer field, the energy resolution depends mostly on E_{tr}, with less influence on ΔV_{MMG}: this explains the reason why energy resolution at first decreases with IBF. On the other hand, for $E_{tr} \geq 250$ V/cm, the energy resolution behaviour is mostly determined by ΔV_{MMG} value. The energy resolution and ion backflow values can be read in Table 9. Even in this case, for $E_{tr} \geq 600$ V/cm, the gain remains constant for further transfer field increase.

7 Summary and Outlook

A hybrid GEM - Micromegas detector, consisting of a GEM (Standard or Large Pitch) and a bulk Micromegas has been assembled and studied.
Energy spectra show that for Standard GEM the electron extraction efficiency reaches the maximum for $E_{\mathrm{tr}} \approx 700$ V/cm (Section 2.2.2).

Studies on the detector gain have revealed an exponential dependence of this quantity on the voltage applied between the MMG and the anode, or between GEM top and GEM bottom. In Section 4.1.1 a comparison between the GEM-Micromegas setup and the single Micromegas detector has been made, showing an increase of the hybrid detector gain of a factor of 10.
Furthermore, when Standard and Large Pitch GEM have been compared, the gain has resulted more in the former case (when $\Delta V_{\mathrm{GEM}} < 200$ V).

The ion feedback has been investigated for different detector configurations. This quantity, mainly determined by the Micromegas voltage, decreases with ΔV_{MMG}, while increases with ΔV_{GEM}, when the gain is kept constant.
It has also been shown that, for 100 V/cm $< E_{\mathrm{drift}} <$ 450 V/cm, IBF increases linearly with the drift field.

Using a ^{55}Fe source, it has been possible to study the energy resolution behaviour. The several scans made, have shown a characteristic anticorrelation between E_{res} and the ion backflow. The only exception is represented by E_{tr} scans, where, within the range of fields and voltages studied, the energy resolution increases with IBF.
The optimal operational region, needed for Hydra experiment, has been reached for a wide range of voltages and fields e.g. for $E_{\mathrm{drift}} = 400$ V/cm; $E_{\mathrm{tr}} = 150$ V/cm; 330 V $< \Delta V_{\mathrm{GEM}} <$ 400 V; 416 V $< \Delta V_{\mathrm{MMG}} <$ 482 V (which correspond to gains between 13600 and 18000).
Due to the larger collection efficiency, it has been confirmed that the Standard GEM exhibits a better energy resolution than the Large Pitch GEM.

In order to quantitatively understand the contribution of the two different amplification stages, the gain of each component could have been measured and compared. Studies show that the total gain can be expressed as the product of the individual stages [16]. According to equation (2), $IBF \cdot G = (1 + \epsilon)$: to verify this dependence, a set of measurements could have been performed, keeping constant the energy resolution.

The hybrid detector offers a wide range of parameters not scanned yet.
The drift and the transfer gaps have been kept constant throughout the entire experiment, respectively to 20 and 4 mm: changing these parameters, additional detector features may be revealed, and the gaps optimum values could be determined. Previous studies showed for instance, that the ion backflow decreases when the drift region increases [27]. The size of the drift gap, on the other hand, has to be large enough to minimise inefficiencies in charged particle detection, but small enough to reduce the dead time due to pulse width.
For further studies, it could be possible to change the gas mixture, e.g. using a Ar Co_2 70-30. Due to the maximum content of ionization component, the gain is expected to be maximum for 90-10 ratio, thus causing less ion feedback. Also, the noble gas Neon, could be used instead of Argon: ion mobility in Ne mixtures is much higher, reducing the size of space-charge distortions by nearly a factor of 2, and increasing the stability against primary discharges [28].
As a next step, the GEM - Micromegas detector performances could been compared with a detector composed of multiple GEMs and a Micromegas: some studies have been already developed with two preamplifier GEMs [16; 26], rotated of 90 degrees

against each other. In such a setup, the second GEM acts to maintain a good energy resolution, and to further block backdrifting ions, with a total gain of about 1.
Furthermore, it is possible to vary the detectors geometry: two different GEMs have been already used, and, subsequently, the results obtained with different Micromegas may be in the future compared. Single Micromegas studies [22] showed for instance that the gain does not depend on the Micromegas geometry, which influences instead its stability.
The location of the source can also be changed: in most experiments, included Hydra, the source of particles is longitudinal with respect to the detectors. The behaviour of the detector with a source hitting from one side, instead of from the top, needs still to be investigated. Furthermore, Hydra experiment plans to use a magnetic field: measurements performed housing the detector inside a magnetic field region will be of fundamental importance in the future.

A satisfying explanation for the trend of energy resolution VS ion backflow presented in Sections 6.3 and 6.4 has not been found yet. Therefore, further measurements needs to be performed, in order to reach a complete understanding of the the hybrid GEM-Micromegas working principles.

8 Appendix

8.1 Alpha spectrum

Figure 28 shows the α energy spectrum. In this case, a noisy spectrum is observed, which makes integration very hard.

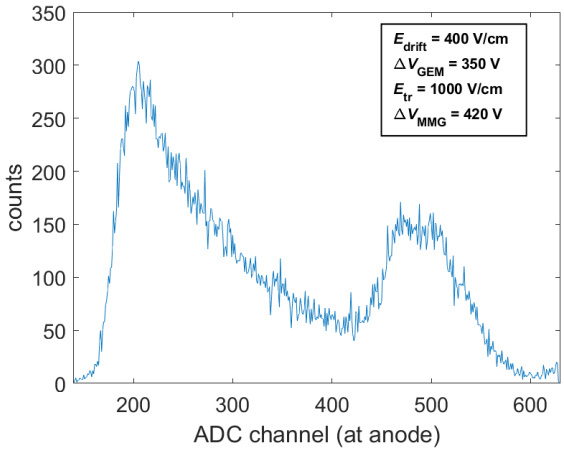

Figure 28: Energy spectra of the α source.

8.2 Currents - ΔV_{GEM} scans

Currents have been measured scanning ΔV_{GEM}, with E_{tr} and $\Delta V_{\mathrm{MMG}} = 0$. Since in the transfer region no electric field is applied, all the electrons created within GEM holes, reach GEM bottom: the currents in GEM top and GEM bottom have the same value, but opposite sign (Figure 30). The amplification occurs for $\Delta V_{\mathrm{GEM}} > 300$ V.

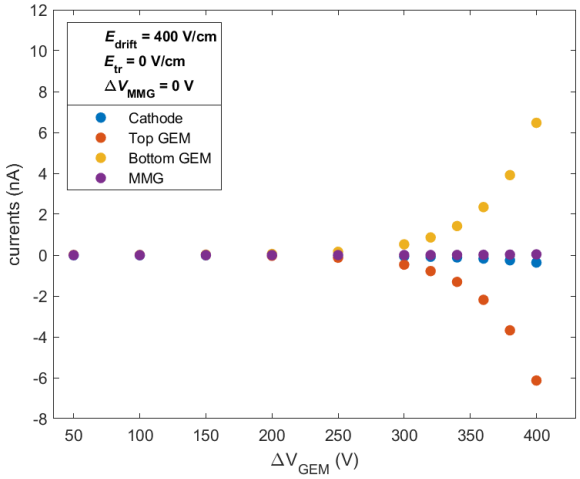

Figure 29: Currents measured scanning ΔV_{GEM}, with $E_{\mathrm{drift}} = 400$ V/cm, $E_{\mathrm{tr}} = 0$ V/cm and $\Delta V_{\mathrm{MMG}} = 0$ V.
Error bars are within the dimension of experimental points.

8.3 Gain as a function of ΔV_{MMG}

G has been calculated for different values of ΔV_{GEM}, when $E_{\mathrm{tr}} = 0$ V/cm. Even in this case, the GEM stage influences the gain, which results more when ΔV_{GEM} increases.

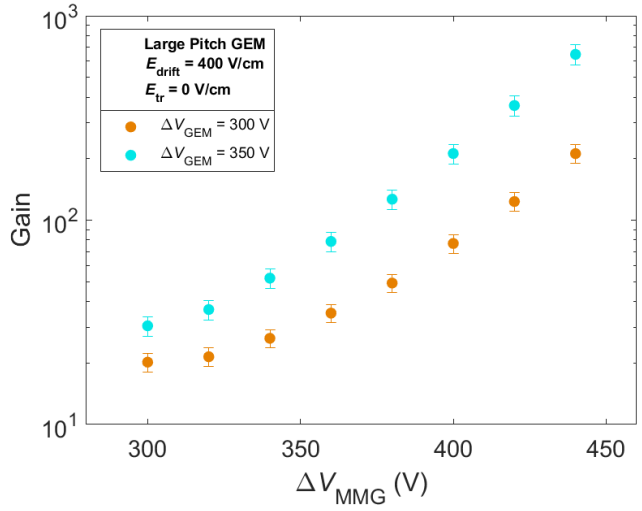

Figure 30: Gain scanning ΔV_{MMG}, for different values of ΔV_{GEM}, with $E_{\mathrm{tr}} = 0$ V/cm.

8.4 Ion backflow as a function of ΔV_{MMG}

IBF has been evaluated scanning ΔV_{MMG}, and keeping the other parameters fixed. The ion backflow decreases with ΔV_{MMG}, until it reaches an asymptotic value (Figure 31). Moreover, *IBF* is more for higher values of E_{tr}, but for $E_{\mathrm{tr}} = 0$ V/cm case.

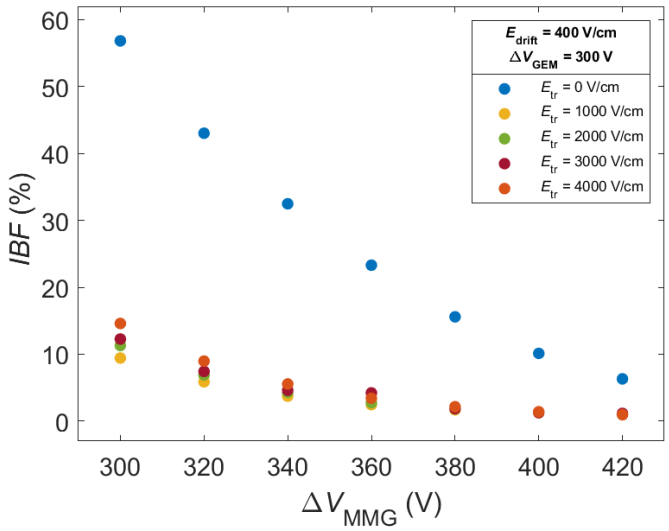

Figure 31: ion backflow as a function of ΔV_{MMG}.
Error bars are within the dimension of experimental points.

8.5 Ion backflow as a function of ΔV_{GEM}

The ion feeback has been studied as a function of ΔV_{GEM}, adjusting the Micromegas voltage. As it can be read in Table 3, in order to keep the gain constant, ΔV_{GEM} increase (10 V) is more than the ΔV_{MMG} decrease ($\approx$ 7 V): this behaviour translates into an overall *IBF* increase (Figure 32). Since higher gain means higher ΔV_{MMG} for the same value of ΔV_{GEM}, the ion backflow is less for larger gain.

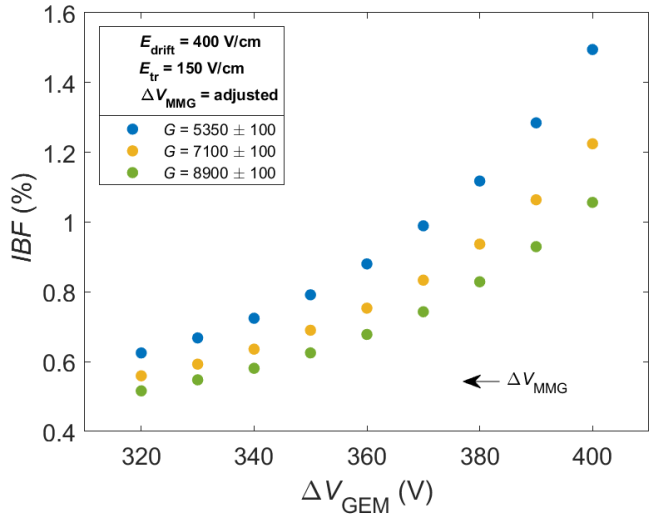

Figure 32: ion backflow as a function of ΔV_{GEM}.
Error bars are within the dimension of experimental points.

ΔV_{GEM} (V) (±1 V)	ΔV_{MMG} (V) (±0.1 V)	*IBF*(%) ($\pm 4 \cdot 10^{-4}$)
320	447.5	0.6250
330	440.0	0.6680
340	432.0	0.7245
350	424.0	0.7916
360	415.6	0.8803
370	407.5	0.9894
380	399.5	1.1178
390	391.0	1.2845
400	382.5	1.4947

(a) Gain = 5350, Standard GEM.

ΔV_{GEM} (V) (±1 V)	ΔV_{MMG} (V) (±0.1 V)	*IBF*(%) ($\pm 2 \cdot 10^{-4}$)
320	457.0	0.5594
330	449.5	0.5929
340	441.8	0.6359
350	434.0	0.6900
360	426.0	0.7534
370	418.1	0.8336
380	409.8	0.9370
390	401.5	1.0640
400	393.0	1.2245

(b) Gain = 7100, Standard GEM.

Table 3: *IBF* values, scanning ΔV_{GEM} and adjusting ΔV_{MMG}, for E_{tr} = 150 V/cm, E_{drift} = 400 V/cm.

8.6 Energy resolution studies - further details

8.6.1 ΔV_{GEM} scans

In GEM voltage scans (E_{drift} = 400 V/cm; E_{tr} = 150 V/cm), the energy resolution improves with ΔV_{GEM}, while the ion backflow increases (Table 4). For the same value of ΔV_{GEM}, the energy resolution is better for higher ΔV_{MMG} (corresponding to higher gains). On the other hand, IBF decreases with ΔV_{MMG}.
Table 4 shows also that the detector gain is mostly provided by the Micromegas: in order to keep the gain constant, when ΔV_{GEM} is increased by 10 V, ΔV_{MMG} needs to be decreased by less than 10 V.

ΔV_{GEM} (V) (±1 V)	ΔV_{MMG} (V) (±0.1 V)	$IBF(\%)$ ($\pm 8 \cdot 10^{-4}$)	E_{res} (%) (±0.4)
330	462.1	0.4860	20.0
340	454.5	0.5217	20.1
350	446.6	0.5652	19.8
360	438.8	0.6137	19.4
370	430.8	0.6708	19.2
380	422.7	0.7503	18.9
390	414.2	0.8450	18.5
400	405.9	0.9559	18.0

(a) Gain = 9130, Standard GEM.

ΔV_{GEM} (V) (±1 V)	ΔV_{MMG} (V) (±0.1 V)	$IBF(\%)$ ($\pm 8 \cdot 10^{-4}$)	E_{res} (%) (±0.4)
330	482.0	0.4217	14.0
340	474.8	0.4418	13.7
350	467.2	0.4654	13.5
360	459.4	0.4944	13.
370	451.4	0.5289	13.1
380	443.4	0.5717	12.7
390	435.4	0.6244	12.6
400	427.3	0.6900	12.5

(b) Gain = 18000, Standard GEM.

Table 4: E_{res} and IBF values, scanning ΔV_{GEM}, for E_{drift} = 400 V/cm, E_{tr} = 150 V/cm.

In Table 5, the energy resolution and ion backflow values are listed, comparing the two GEMs. In order to obtain the same gain of 13600, in the Standard GEM ΔV_{MMG} has to be higher, meaning better energy resolution and less IBF.

ΔV_{GEM} (V) (±1 V)	ΔV_{MMG} (V) (±0.1 V)	$IBF(\%)$ ($\pm 4 \cdot 10^{-4}$)	E_{res} (%) (±0.3)
330	471.4	0.4521	15.0
340	464.0	0.4766	14.7
350	456.4	0.5048	14.1
360	448.5	0.5447	13.8
370	440.6	0.5843	13.7
380	432.5	0.6394	13.6
390	424.3	0.7092	13.5
400	416.0	0.7928	13.2

(a) Gain = 13600, Standard GEM

ΔV_{GEM} (V) (±1 V)	ΔV_{MMG} (V) (±0.1 V)	$IBF(\%)$ ($\pm 3 \cdot 10^{-4}$)	E_{res} (%) (±0.3)
330	445.5	0.6608	13.4
340	437.0	0.7274	13.3
350	429.0	0.8034	13.0
360	420.3	0.9080	12.9
370	411.7	1.0366	12.9
380	403.0	1.1976	12.9
390	394.0	1.4081	12.8
400	385.0	1.6765	13.0

(b) Gain = 13600, Large Pitch GEM

Table 5: E_{res} and IBF values, scanning ΔV_{GEM} with Standard and Large Pitch GEM, for E_{drift} = 400 V/cm, E_{tr} = 150 V/cm.

8.6.2 E_{drift} scans

Table 6 shows energy resolution and ion backflow values, for E_{drift} scans, $E_{\text{tr}} = 150$ V/cm and $\Delta V_{\text{MMG}} = 430$ V. In this case, ΔV_{GEM} varies slightly, and thus E_{res} remains almost constant. The ionbackflow increases with E_{drift}, as expected. For the same value of E_{drift}, IBF results independent of ΔV_{GEM}: it varies (either increasing or decreasing) of only $\approx 1\%$ for a variation of 10 V on the GEM voltage. This result demonstrates that the ion backflow depends mostly on E_{drift} value, and less on ΔV_{GEM}.

E_{drift} (V/cm) (±1 V)	ΔV_{GEM} (V) (±0.1 V)	$IBF(\%)$ ($\pm 4 \cdot 10^{-4}$)	E_{res} (%) (±0.3)
100	395.7	0.2360	12.2
150	396.3	0.3312	11.9
200	396.8	0.4220	11.7
250	397.3	0.4907	11.7
300	397.5	0.5660	11.5
350	397.6	0.6240	11.4
400	397.5	0.6895	11.4
450	397.5	0.7434	11.3
500	397.4	0.7961	11.4

(a) Gain = 16900, Standard GEM

E_{drift} (V/cm) (±1 V)	ΔV_{GEM} (V) (±0.1 V)	$IBF(\%)$ ($\pm 3 \cdot 10^{-4}$)	E_{res} (%) (±0.3)
100	405.0	0.2347	12.2
150	406.0	0.3323	11.6
200	406.5	0.4173	11.5
250	406.8	0.4949	11.3
300	407.1	0.5626	11.3
350	407.2	0.6264	11.1
400	407.3	0.6832	11.2
450	407.3	0.7408	11.0
500	407.7	0.8058	11.1

(b) Gain = 21200, Standard GEM

Table 6: E_{res} and IBF values, scanning E_{drift}, for $E_{\text{tr}} = 150$ V/cm, $\Delta V_{\text{MMG}} = 430$ V.

In E_{drift} scans case, for the same value of IBF the Large Pitch GEM energy resolution results worse than the Standard one (Figure 33).

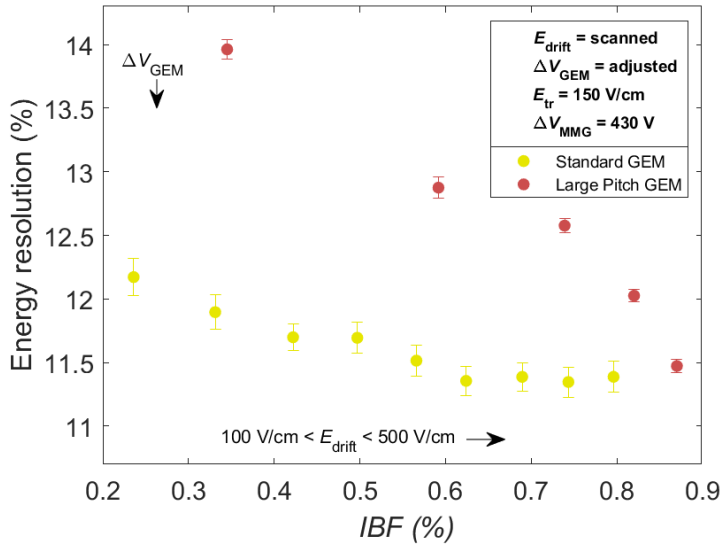

Figure 33: energy resolution as a function of ion backflow, for E_{drift} scans. Comparison between Standard and Large Pitch GEM.

8.6.3 E_{tr} scans

Table 7 shows E_{res} and IBF values for transfer field scan, adjusting ΔV_{GEM}. Energy resolution deteriorates as E_{tr} increases, since ΔV_{GEM} gets smaller (up to E_{tr} = 600 V/cm). IBF, which depends most on E_{tr}, increases, despite the ΔV_{GEM} reduction.

E_{tr} (V/cm) (±1 V)	ΔV_{GEM} (V) (±0.1 V)	IBF(%) ($\pm 4 \cdot 10^{-4}$)	E_{res} (%) (±0.4)
200	375.0	0.7301	13.7
250	371.5	0.8009	13.9
300	366.5	0.8549	14.4
400	361.5	0.9481	15.6
500	359.0	1.0229	17.1
600	358.2	1.0794	18.3
700	358.3	1.1163	19.0
800	358.2	1.1163	19.4
1000	358.5	1.1321	20.5

(a) Gain = 12500, Standard GEM

E_{tr} (V/cm) (±1 V)	ΔV_{GEM} (V) (±0.1 V)	IBF(%) ($\pm 4 \cdot 10^{-4}$)	E_{res} (%) (±0.4)
200	387.4	0.7552	12.4
250	382.0	0.8038	12.9
300	378.0	0.8580	14.0
400	372.8	0.9505	15.7
500	370.3	1.0299	17.2
600	369.5	1.0856	18.4
700	369.5	1.1285	19.1
800	369.5	1.1405	19.4
1000	369.8	1.1553	19.6

(b) Gain = 15700, Standard GEM

Table 7: E_{res} and IBF values, scanning E_{tr}, and adjusting ΔV_{GEM}, for E_{drift} = 400 V/cm, ΔV_{MMG} = 430 V.

In E_{tr} scans using Large Pitch GEM, E_{res} follows an irregular trend when studied as a function of ion backflow, at odd with Standard GEM behaviour (Figure 25).

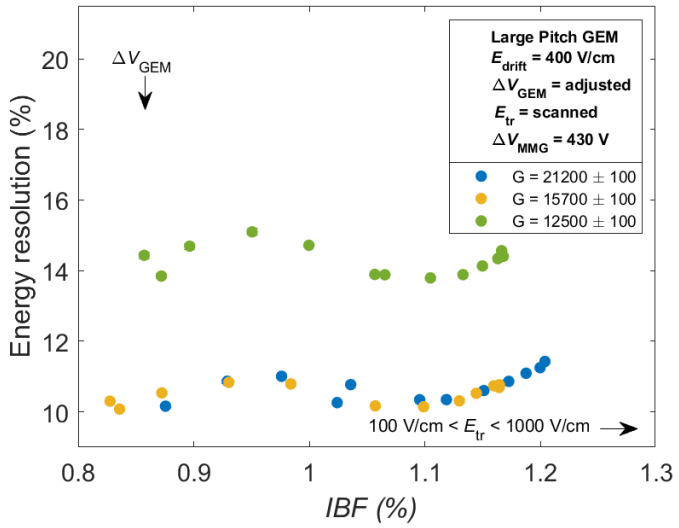

Figure 34: energy resolution as a function of ion backflow, for E_{tr} scans, with LP GEM. Error bars are within the dimension of experimental points.

Here a comparison between Standard and Large Pitch GEM values is shown (Table 8). In Standard case, as already discussed, the energy resolution gets worse as ΔV_{GEM} decreases. For LP GEM, on the contrary, the energy resolution neither decreases nor increases, but rather oscillates around a value of 10%. *IBF* behaviour though, meets the expectations, being more for Large Pitch GEM, and increasing with E_{tr}.

E_{tr} (V/cm) (±1 V)	ΔV_{GEM} (V) (±0.1 V)	$IBF(\%)$ $(\pm 4 \cdot 10^{-4})$	E_{res} (%) (±0.4)
200	387.4	0.7552	12.4
300	378.0	0.8580	14.0
400	372.8	0.9505	15.7
500	370.3	1.0299	17.2
600	369.5	1.0856	18.4
700	369.5	1.1285	19.1
800	369.5	1.1405	19.4
1000	369.8	1.1553	19.6

(a) Gain = 15700, Standard GEM

E_{tr} (V/cm) (±1 V)	ΔV_{GEM} (V) (±0.1 V)	$IBF(\%)$ $(\pm 1 \cdot 10^{-4})$	E_{res} (%) (±0.1)
200	350.0	0.8723	10.5
300	339.5	0.9839	10.8
400	337.0	1.0570	10.2
500	338.0	1.0988	10.1
600	340.5	1.1297	10.3
700	343.0	1.1444	10.5
800	346.0	1.1595	10.7
1000	350.0	1.1643	10.8

(b) Gain = 15700, Large Pitch GEM

Table 8: E_{res} and *IBF* values, scanning E_{tr}, and adjusting ΔV_{GEM} with Standard and Large Pitch GEM, for E_{tr} = 400 V/cm, ΔV_{MMG} = 430 V.

Table 9 refers to E_{tr} scans, adjusting ΔV_{MMG}. In this case, first energy resolution improves as E_{tr} increases and ΔV_{MMG} gets smaller: supposedly, in this range, E_{tr} plays a more important role than ΔV_{MMG}, in determining E_{res} values. After the minimum (when E_{tr} = 250 V/cm) is reached, the energy resolution gets worse at increasing values of the transfer field. On the other hand, *IBF* increases with E_{tr}, as expected. For the same value of the transfer field, the ion backflow is more when ΔV_{MMG} decreases.

E_{tr} (V/cm) (±1 V)	ΔV_{MMG} (V) (±0.1 V)	$IBF(\%)$ $(\pm 7 \cdot 10^{-4})$	E_{res} (%) (±0.3)
150	440.0	0.6525	13.2
200	434.5	0.7403	12.4
250	430.0	0.8194	11.9
300	427.0	0.8916	12.3
400	423.0	1.0080	14.3
500	421.0	1.0911	16.4
600	420.5	1.1451	17.2
800	421.0	1.1858	18.2
1000	421.5	1.1938	18.9

(a) Gain = 12500, Standard GEM

E_{tr} (V/cm) (±1 V)	ΔV_{MMG} (V) (±0.1 V)	$IBF(\%)$ $(\pm 7 \cdot 10^{-4})$	E_{res} (%) (±0.3)
150	450.0	0.5773	14.3
200	445.0	0.6663	13.0
250	440.0	0.7542	12.5
300	436.5	0.8214	12.6
400	433.0	0.9392	13.3
500	431.0	1.0245	15.1
600	430.0	1.0864	16.1
800	430.0	1.1323	17.4
1000	430.0	1.1347	18.2

(b) Gain = 15700, Standard GEM

Table 9: E_{res} and *IBF* values, scanning E_{tr}, and adjusting ΔV_{MMG}, for E_{drift} = 400 V/cm, ΔV_{GEM} = 370 V.

9 Acknowledgments

First of all, I would like to thank Dr. Piotr Gasik, for all the things he taught me during these months, the constant patience he had, and the feedback I always received from his side. Without him and his enormous experience on GEMs, nothing of this would have been possible.
I couldn't thank enough Berkin Ulukutlu, who daily helped me (even when he was at Cern), giving me suggestions and inspirations for the experiment. He had great patience and enthusiasm, and always answered all the questions I had. I learnt so much from him.
I want to thank Tobias Waldmann, who helped me during the measurements. Thank to him I felt comfortable in the lab from the first day I arrived. Thank also to Thomas Klemenz, who was ready to help me whenever I asked.
And of course thank to Prof. Laura Fabbietti, who accepted me within her joyful group lab, giving me opportunities that I could never have imagined, and constantly supporting me. I feel contemporary very lucky and grateful.

On the Italian side, thank to Prof. Alessandro De Falco, for reviewing this thesis and the helpfulness he always had.
I must thank my two lab friends, Elisa Pili and Elisabetta Mereu, who always have been of great support along these three university years, and put up with me and my mood: thank to you, I learnt how working on a lab group means.

Finally, thank to my family (especially to my dad who helped me with the aesthetic part of this thesis) and to all my friends, who always believed in me and cheered me up.

References

[1] F. Sauli. Gaseous Radiation Detectors. *Cambridge Univertsity Press, Cambridge, 2014.*

[2] Glenn F Knoll. Radiation detection and measurement. *John Wiley and son, 2000,* ISBN 0-471-07338-5.

[3] Ahmed, Syed (2007). Physics and Engineering of Radiation Detection. Elsevier. Bibcode:2007perd.book A. ISBN 978-0-12-045581-2.

[4] Pinto, S.D. Micropattern gas detector technologies and applications, the work of the RD51 collaboration. *IEEE Nuclear Science Symposium 2010 Conference Record,* arXiv:1011.5529.

[5] `https://cernbox.cern.ch/index.php/s/UZeVxEIuly0TpEk/download`

[6] Physics and Engineering of Radiation Detection. Syed Naeem Ahmed. *Queen's University, Kingston, Ontario*, E.1, Intrinsic Energy , p. 260.

[7] F. Sauli. The gas electron multiplier (GEM): Operating principles and applications. *Nuclear Instruments and Methods in Physics Research,* A 805 (2016) 2–24.

[8] F. Sauli. GEM: A new concept for electron amplification in gas detectors. *Nuclear Instruments and Methods in Physics Research,* A 386 (1997) 53 l-534.

[9] K. Dehmelt, P. Garg, T. K. Hemmick, A. Milov, E. Shulga, V. Zakharov. Passive Gating Grid for Ion Back Flow Suppression in High Luminosity Collider Experiments. *Instrumentation and Detectors (physics.ins-det); Nuclear Experiment (nucl-ex)*, arXiv:1912.12247 [physics.ins-det].

[10] I. Giomataris, Ph.Rebourgeard, J.P.Robert, G.Charpak. MICROMEGAS: a high-granularity position-sensitive gaseous detector for high particle-flux environments. *Nuclear Instruments and Methods in Physics Research,* A 376 (1996) 29-35.

[11] D. Attié, S. Aune, E. Berthoumieux , F. Bossù , P. Colas, A. Delbart, E. Dupont, E. Ferrer Ribas, I. Giomataris , A. Glaenzer, H. Gómez, F. Gunsing, F. Jambon, F. Jeanneau, M. Lehuraux, D. Neyret, T. Papaevangelou, E. Pollacco, S. Procureur, M. Revolle, P. Schune, L. Segui, L. Sohl, M. Vandenbroucke, Z. Wu. Current Status and Future Developments of Micromegas Detectors for Physics and Applications. *Applied Sciences* - 2.Micromegas Fabrication Techniques.

[12] P. Colas, I. Giomataris, V. Lepeltier. Ion backflow in the Micromegas TPC for the future linear collider. *Nuclear Instruments and Methods in Physics Research,* A 535 (2004) 226–230.

[13] H. Raether. Electron avalanches and breakdown in gases. *1964*.

[14] S. Yu-Lian, Q. Hui-Rong, H. Bi-Tao, F. Sheng-Nan, W. Bo, L. Mei, Z. Jian, L. Rong-Guang, C. Guang-Cai, L. Peng, O. Qun, C. Yuan-Bo, Y. Fu-Ting. Investigation of GEM-Micromegas detector on x-ray beam of synchrotron radiation. *Chinese Physics*, C Vol. 33, No. X, Xxx, 2009.

[15] S. Kane, J. May, J. Miyamoto, I. Shipsey, S. Andriamonje, A. Delbart, J. Derre, I. Giomataris, F. Jeanneau. A study of Micromegas with preamplification with a single GEM. *Advanced Technology and Particle Physics*.

[16] V. Ratza, M. Ball, M. Liebtrau, B. Ketzer. Characterization of a hybrid GEM-Micromegas detector with respect to its application in a continuously read out TPC. *EPJ Web of Conferences*, 174, 01016 (2018).

[17] P. Gasik, A. Mathis, L .Fabbietti, J. Margutti. Charge density as a driving factor of discharge formation in gem-based detectors. *Nuclear Instruments and Methods in Physics Research Section A: Accelerators, Spectrometers, Detectors and Associated Equipment*, 870:116–122, 2017.

[18] `https://indico.gsi.de/event/11513/contributions/48486/attachments/33229/42910/HYDRA_GSIworkshop_Oct2020.pdf`

[19] `https://ep-dep-dt.web.cern.ch/micro-pattern-technologies`

[20] Particle Detectors at Accelerators. *34.2.2 Gaseous photon detectors*.

[21] S. Bachmann, A. Bressan, L. Ropelewski, F. Sauli, A. Sharma, D. MoKrmann. Charge amplification and transfer processes in the gas electron multiplier. *Nuclear Instruments and Methods in Physics Research*, A 438 (1999) 376-408.

[22] T. Waldmann. Electrical and optical discharge studies with various mpgds. *Bachelor Thesis, Munich, 2020*.

[23] V. Ratza. Multi-stage Micropattern Gaseous Detectors for the ALICE TPC Upgrade - Studying and Modelling Charge Transfer and Energy Resolution. *Dissertation zur Erlangung des Doktorgrades*.

[24] M. Ball, J. Bloemer. Parametrisation of extraction and collection efficiencies. *Status report*.

[25] The upgrade of the ALICE TPC with GEMs and continuous readout. *ALICE TPC collaboration et al 2021 JINST 16 P03022*.

[26] S. Aiolaa, R.J. Ehlersa, S. Gua, J.W. Harrisa, R. Majkaa, J.D. Mulligana, M. Olivera, J. Schambachb, N. Smirnova. Combination of two Gas Electron Multipliers and a Micromegas as gain elements for a time projection chamber. *arXiv:1603.08473v1 [physics.ins-det]*, 28 Mar 2016.

[27] M. Ball, K. Ecksteina, T. Gunji. Ion backflow studies for the ALICE TPC upgrade with GEMs. *3rd International Conference on Micropattern Gaseous Detectors 1-6 July, 2013, Zaragoza, Spain*.

[28] ALICE Collaboration. *TDR for the Upgrade of the ALICE TPC* (CERN/LHCC, Geneva, 2014).